Chapter 14

Lithium Niobiosilicate Glasses Thermally Treated

Manuel Pedro Fernandes Graça and Manuel Almeida Valente

Additional information is available at the end of the chapter

http://dx.doi.org/10.5772/50243

1. Introduction

The term glass comes from the latin word, vitrium, and refers to one of the oldest known material. It is defined in accordance with the ASTM C-169-92 norm, as an inorganic product obtained by quenching a melt until hardness conditions, without crystallization. This definition is however too restrictive because it only applies to glasses prepared by fusion method. A broader definition is that proposed by A. Paul: the glass shows the elastic behavior characteristic of the crystalline state and the behavior of the viscous liquid state. The most common properties of the glasses are the transparency to visible radiation, mechanical stability, inert at the biological level and dielectric material. However, due to the possibility of controlling the microstructure by changing the composition or by applying heat treatments, controlling the process of nucleation and crystallization, the properties of glasses can be modified.

The initial chemical composition is a factor, controllable, which allows to shape some of the properties of the glasses. In any glass, the units that define its structure can be divided into three categories, defined according to their structural function, network former; modifier and intermediate species. The formers are units that, without the addition of other elements, can form glass such as SiO_2, B_2O_3, GeO_2 and P_2O_5. The network modifiers, do not form glass by itself, but are often combined with a former. Examples of modifying elements are the alkaline elements (Li, Na, K, etc.) and alkaline-earth metals (Mg, Ca, etc.). The intermediate species are elements that can both play a role in forming or modifying the network (Al, Nb, etc.).

The formation of glass ceramics, for example by heat treatment of the as-prepared glass, shows at the technological level great advantages, for the single crystals and sintered ceramics, as the possibility of their properties (optical, electrical, mechanical, chemical, etc.) be controlled via the volume fraction of the active phase dispersed in the matrix. For example, to maintain optical transparency, the process of nucleation and crystal growth

requires a great degree of control being achieved when the size of the crystals dispersed in the glassy matrix is not high enough to cause light scattering. However, for most electrical applications it is necessary that the crystals are large enough to present, for example, a ferroelectric response. This commitment is not easy to perform. Another condition that can maintain the optical transparency of a glass ceramic is the small difference between the refractive indices of the crystals and of the glassy matrix. If this difference is insignificant it allows, regardless of the size of the crystals, to keep the optical transparency. In recent years there has been a growing interest in the preparation, characterization and technology implementation of glasses and glass ceramics in different type of devices. However, it is important to note that, in general, the electrical and optical properties of glass ceramics are not as good as their single crystal when not embedded in a matrix. This is due to the fact that the glass ceramics present at least two distinct phases, the crystal (considered the active phase) and the amorphous (support). The electric polarization of the crystals embedded in a glassy matrix is more difficult due to the low value of the dielectric constant of the glassy phase. On the other hand and because of the single crystal growth processes present a high economic cost, have now start to been replaced by glass ceramics. Some glass ceramics have the additional advantage of being dense and not porous materials.

The growth and crystal orientation can generally be achieved through different processes, such as: mechanical deformation, thermodynamic control, kinetic control (electrochemical induced nucleation). In glasses the use of thermodynamic control is the most common. However, control of crystallization, with the desired crystalline phase is usually difficult because crystallization is a complex process affected by various factors such as composition, surface conditions and heat treatment parameters.

The crystallization process, in a glass, of a particular crystalline phase oriented in a pre-defined direction is usually a desirable objective but difficult to implement. One way that can induce the crystallization of oriented particles in a glass is the application, together with the thermal process of external fields (magnetic / electric). In the presence of an electric field polar nuclei should be oriented parallel to the field and the existing nuclei and / or crystallites can rotate until reach the same direction. However, this can only occur if the value of the electric field is high enough to allow the resultant force to overcome the viscous medium, enabling the rotation. Currently, glass ceramics containing ferroelectric crystals are a class of materials with high technological interest because of the ferroelectric crystals presenting a structural anisotropy results in the formation of electric dipoles and therefore a spontaneous electric polarization.

A large number of ferroelectric materials is presented in the form of crystalline ceramic. The scientific and technological development that photonics has been presenting, has required, particularly in terms of applications, new materials which exhibit characteristics such as optical transparency and are optically active so they can be used as amplifiers, switches, sensors, transducers, filters (…) , that is because there is a need for materials that use light to perform functions already implemented in electronic devices (mainly in the sectors of communications, energy, instrumentation, etc.), but more efficiently or giving rise to new

devices. Thus the preparation, structural, electrical and optical characterization of glass ceramic showing ferroelectric properties is of great importance for potential technological applications.

Of the various ferroelectric known materials, lithium niobate ($LiNbO_3$), first synthesized in 1949 by Matthias and Remeika, had attracted attention from many researchers due to their excellent piezoelectric properties, electro optics, electroacoustic, pyroelectric and photorefractive. In late 1960, due to the appearance and development of various applications of fiber optics, several research centers, including Bell Laboratories, studied in detail the structural characteristics and properties of $LiNbO_3$ crystal, especially its electro optics properties.

The fact that the preparation of $LiNbO_3$ single crystals, by the traditional growth techniques is technically difficult and economically costly, the scientific research about the preparation methods of inorganic glasses containing $LiNbO_3$ crystals is the main topic of this chapter. Their structural, morphological, optical and electrical properties will be discussed in function of the glass treatment parameters.

The as-prepared glasses were prepared by sol-gel method. This method allowed to prepare glasses of molar composition $(100-2x)SiO_2\text{-}xLi_2O\text{-}xNb_2O_5$, with $x < 10$, that through the melt-quenching method are of extreme difficulty to prepare. The synthesis of the glass ceramics was performed by heat treatment of the as-prepared glass and the nucleation and growth of crystals in the glass matrix controlled by the heating rate, temperature and treatment time. It was introduced for the first time, a new variable in this type of glass treatments that was the presence of a external dc electric field, during the heat-treatment cycle.. These heat treatments, with external electrical field applied treatments were called thermoelectric (TET). The main objective of the TET is the hypothesis of promote the precipitation of nano-size crystals in a crystalline preferred orientation. In all prepared compositions, $LiNbO_3$ particles were precipitated due to the thermal treatments, in the glass surfaces. The electric analysis showed the presence of conduction, relaxation and polarization mechanisms.

2. Preparation of glasses by the Sol-Gel method

In the literature there is a considerable number of works on the preparation of glasses by melt-quenching. However, it does not exist, to our knowledge, a comparable number of publications on the same type of glasses prepared by sol-gel method. The preparation of materials by sol-gel, with relevant scientific and technological characteristics only began after 1930. However this method was discovered in late 1800. It was, only, after 1970, and with the preparation of inorganic monolithic gels and their subsequent thermal treatment, resulting in glasses, that this method start to developed [1-2].

The sol-gel method has opened a new path for the preparation of glasses of high technological interest, presenting a high degree of chemical purity and very high homogeneity. The preparation of a glass according to this method is performed by mixing, in the liquid state, its constituents until a homogeneous solution, at the molecular level, is

reached. It is then subjected to polymerization and gelling (gel point is defined as the point, in time, where the mixture forms a rigid substance and can be removed from the original container [3]). The resulting gel is transformed into glass by heat treatment during which the volatile species are eliminated and the material undergoes a densification [4]. This method of preparation is known by the generic name sol-gel process. In this process there are two variants, which have the common passage through a gel phase (forming a 3D network [1]) but which differ in the starting products and the first steps of reaction. In one, it starts with a colloidal suspension and in the other with metal-organic compounds, which are dissolved in alcohols. Indeed, the scientific name sol-gel process can only be applied to the first case but it is also used to the second [4;5].

The method using solutions of polymerizable species, which was used in the preparation of the gels presented in this chapter, starts with liquids or alcoholic solutions of an organometallic compound such as the metal alkoxides M(OR)n, where M is a metal and R an alkyl group, exposing them to reactions of hydrolysis, polymerization and dehydration [3;6]. In this method, the alkoxides usually used are the tetraethylorthosilicate (TEOS) and the tetrametoxisilicate (TMOS). However, in several papers other type of alkoxides can be found, such as boron, aluminum or titanium but, usually, mixed with the TEOS. In the case of the gels prepared in this work, the TEOS solution was the only used and the remained components were introduced in the form of nitrate ($LiNO_3$) and chloride ($NbCl_5$), mainly due to their high solubility in water and/or alcohol.

Regarding the chemical formation of a polymeric gel from metal alkoxides (M (OR) n), it is typically described by two consecutive reactions:

- hydrolysis ($M(OR)_n + xH_2O \rightarrow M(OH)_x(OR)_{n-x} + xROH$)

and the condensation, which can be subdivided into two phases:

- alcohol condensation ($-M-OH+R-O-M \rightarrow -M-O-M- \quad +ROH$)
- and water condensation ($-M-OH+H-O-M \rightarrow -M-O-M- \quad +H_2O$) [1;4;5].

Briefly, the hydrolysis reaction is the substitution of the alkoxy group (OR) with a hydroxide group (OH). The subsequent condensation reactions involves, in the case of TEOS ($Si(OC_2H_5)_4$), the silanol group (Si-OH) that gives rise to siloxane bonds Si-O-Si), water and alcohol. It must be noticed that these reactions are, however, a simplified version of which occurs during the hydrolysis and condensation of the alkoxide solutions [4;5].

The diagram showed in figure 1 represents, according to Sakka et al. [6], the preparation of a glass from metal alkoxides. This diagram shows the preparation of a binary glass of the SiO_2-TiO_2 system. The treatment temperatures found in the flowchart are only examples, because they depend directly on the glass composition.

According to figure 1, the preparation process can be divided into three steps. The first involves the mixing of the alkoxide in the amounts corresponding to the final composition of the glass, yielding a clear solution. In the second step it is added to the alkoxide solution

water, alcohol and acid to induce the hydrolysis. Parameters such as the pH, the molar ratio between H_2O and the alkoxide and the presence of catalysts (acids) may, as desired, that the onset of condensation is given only after the end of the hydrolysis of the metal alkoxide. In addition to this fact and due to the immiscibility between the water and the alkoxide it is necessary to use a mutual solvent, such as ethanol (C_2H_5OH). The reactions of hydrolysis and polymerization induce an increase of the solution viscosity until it becomes a gel. In the third stage the gel is heat treated until be converted into a glass [2;6].

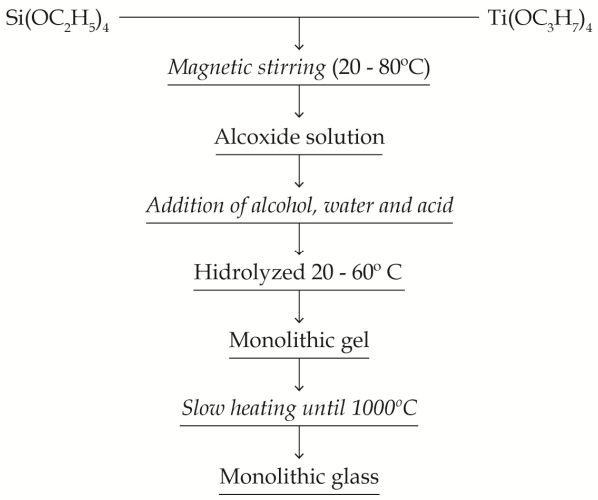

Figure 1. Flowchart of the sol-gel process used in the formation of a SiO_2-TiO_2 glass [6].

With this sol-gel process it is possible to have a high control in the interaction between the liquid precursors, minimizing the energy required for the process, obtaining a final product with high homogeneity and with a high control of its morphology [7]. In summary, the major advantages of this sol-gel process are the high purity of the end product, the low temperature processing (these characteristics are related to the nature of the starting materials), high homogeneity, novel compositions, which are very difficult or even impossible to synthesize by other processes [7;8] and the ability of the shape of final products to be wide (thin film, monolithic blocks, fibers, beads and powders) [6;9;10;11;12].

The major disadvantage of the sol-gel method, for the preparation of glasses, when compared to the melt quenching method (traditional method for glass preparation), is the high cost of starting materials, namely the metal alkoxides [7;8].

A major problem related with the preparation of monolithic blocks is the shrinkage of the gel during the drying process, leading to very high internal mechanical stresses and therefore fracture of the block can occur [13]. This shrinkage is related to the removal of fluids which are inside the pores, resulting in a stress on the capillary walls, which is inversely proportional to the pore diameter [14]. One way to minimize the gel fracture is to

control the drying process. For example, Chou et al. [13] present a thermal process in which includes: (a) removal of ethanol (50 °C), water (90 °C, 4h), formamide (170 °C, 4h) and glycerol (230 °C, 14-18h); (2) burning of organic waste; (3) elimination of pores.

The heating rate, usually less than or equal to 5 °C/min, the treatment temperature and the treatment duration time are critical factors that must be control, to prevent fracture. Furthermore, the use of long treatment times, at or near room temperature (20-50 °C), promote poly-condensation, which is an advantage to produce gels with well-defined microstructure, reducing the stresses [13]. Another important factor is to control the thickness of the gel. The greater the thickness of the gel greater the time required to complete the reaction [3-5]. The transition from gel to glass is usually accompanied through drying and sintering by an appropriate heat treatment process [2;13]. This process depends on the composition.

3. Preparation of SiO_2-Li_2O-Nb_2O_5 glasses by sol-gel – Experimental description

The sol-gel method was used to prepare clear glasses of the ternary system SiO_2-Li_2O-Nb_2O_5. The choice of the molar compositions was based on the following criteria: equal molar amounts of lithium oxide and niobium oxide; obtain a clear gel. In this method, the starting materials were the lithium nitrate ($LiNO_3$), niobium chloride ($NbCl_5$), hydrogen peroxide (H_2O_2 - 30% V/V), tetraethylorthosilicate (TEOS) and ethanol (C_2H_5OH) as the mutual solvent.

The preparation steps are presented in the diagram of figure 2.

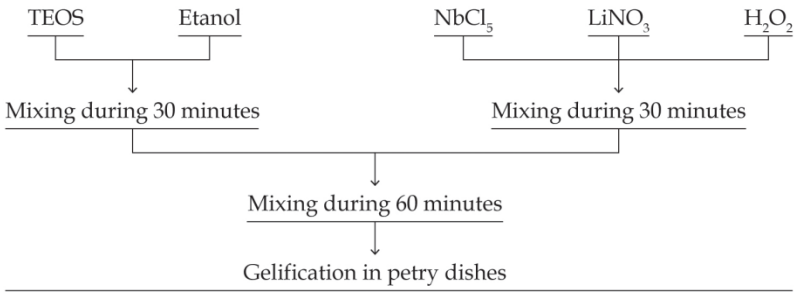

Figure 2. Diagram of the method used to prepare the glasses [16;17].

All samples were prepared using a molar ratio between $(C_2H_5O)_4Si$: C_2H_5OH : H_2O_2 of 1:3:8. Hydrogen peroxide (H_2O_2) was used in the form of aqueous H_2O_2 (3% V/V). This dilution was carried out using deionized water. All solutions, placed in petri boxes were left to gelling at a constant temperature of 30 °C, during more than 1 week. The gel was submitted to a heat treatment which gave rise to the as-prepared sample. This treatment (Fig.3) consists of two steps. First, at a temperature of 120 °C for 48 °C, with the purpose of release the maximum number of free H_2O groups. The second stage has two heat levels.

The first at 250 °C, with the purpose of releasing some H_2O groups, that probably still exist [4;5] and the second, at 500 °C, whose main aim is the liberation of the CO_2 groups from the oxidation of organic radicals [nav91; sil90] . For this reason the heating rate must be as slow as possible.

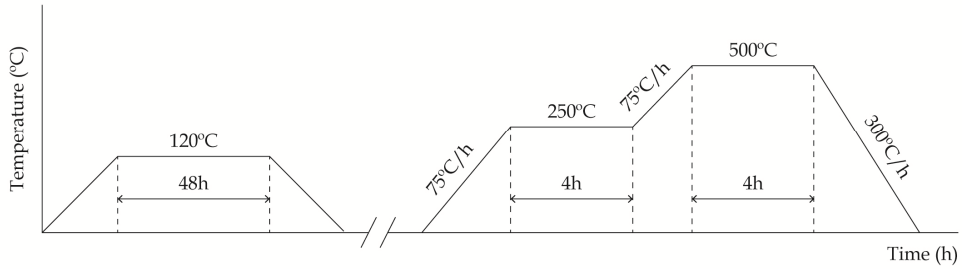

Figure 3. Diagram of the drying process.

4. Glass-ceramics preparation

4.1. Thermal treatments (TT)

The dried gels were submitted to heat treatments in order to obtain glass-ceramics with the $LiNbO_3$ crystalline phase. It is important to refer that the samples prepared by this method present a thickness of 1 mm, approximately. Figure 4 depicts the profile of the heat treatment used. These treatments were performed in a horizontal tube furnace. The value of the threshold temperature parameter (T_P) was chosen based on the information obtained from the thermal analysis of each composition. This thermal analysis was performed using a Linseis Aparatus [18].

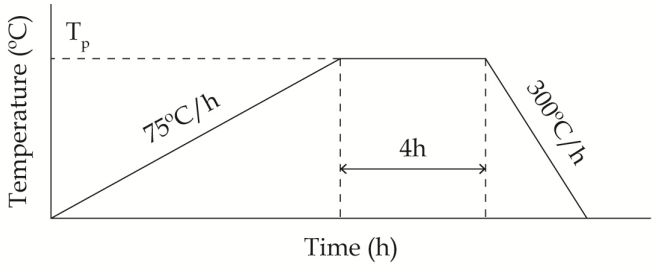

Figure 4. Diagram of the thermal treatment process.

4.2. Thermoelectric treatments (TET)

The heat treatments with the presence of an external electrical field, named as thermoelectric treatment, were carried out in a vertical tube furnace, designed and constructed for this purpose. Figure 5 shows a schematic draw of the oven.

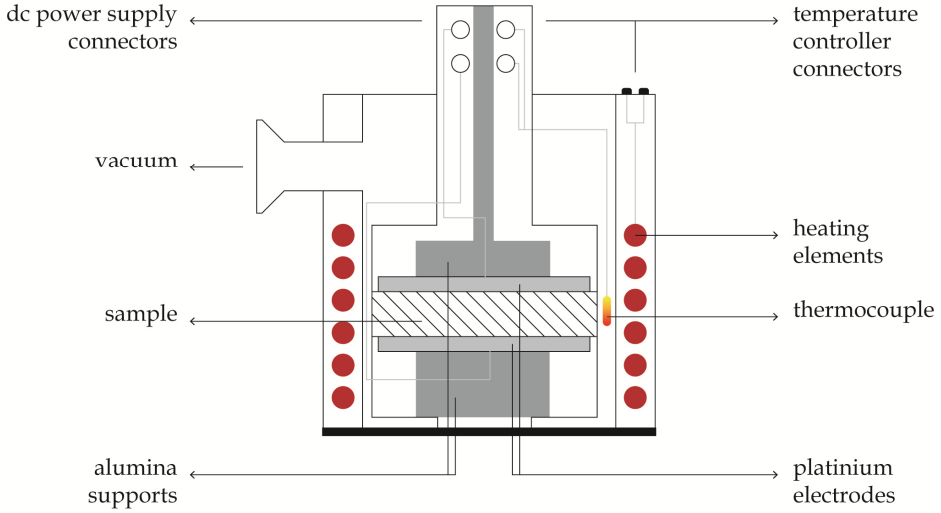

Figure 5. Schematic draw of the oven used for the thermoelectric treatments [19].

The dc external electric field was produced using a high dc voltage source (PS325 Stanford Research System), which could apply a potential difference between 25 V and 2500 V, with a maximum current of 10.5 mA. The temperature was controlled by a Digi-Sense Temperature Controller R/S. All the treatment process is controlled by computer. In these treatments, the thermoelectric cycles used (heating ramp, threshold temperature, treatment time and cooling ramp) were equal to those used in the treatments without the presence of an external field (horizontal tube furnace). In the TET treatments the dc electric field was applied during the periods of heating and dwell, and switched off at the beginning of the cooling step. The parameters: temperature level (T_P) and electric field amplitude are specified and justified in following sections.

5. Samples composition

By the sol-gel method the following two compositions were prepared:

- $92SiO_2$-$4Li_2O$-$4Nb_2O_5$ (mole%);
- $88SiO_2$-$6Li_2O$-$6Nb_2O_5$ (mole%);
- $84SiO_2$-$8Li_2O$-$8Nb_2O_5$ (mole%);

referenced from here by 92Si, 88Si and 84Si, respectively. The 84Si composition did not form a transparent and amorphous gel and glass, indicating the composition limit for those characteristics. This composition was therefore not full characterized.

The preparation process of the glasses and glass ceramics, the results of structural and electrical analyzes and their discussion, are the following sections.

6. Samples preparation

The preparation of the based glass with molar composition $92SiO_2$-$4Li_2O$-$4Nb_2O_5$ and $88SiO_2$-$6Li_2O$-$6Nb_2O_5$ followed the procedure described in figure 2. With the aim of obtain glass ceramics containing $LiNbO_3$ crystallites, heat treatments (TT) were carried out on the as-prepared glass samples (treated at 120 ° C for 48 h and subsequently at 500 ° C for 4 h), which present a thickness between 0.6 and 1.0 mm. For the TT, carried out in a horizontal tubular furnace, the threshold temperature (T_p) choice, differential thermal analyzes (DTA) was performed to the base glass of each composition. The temperatures at the observed exothermic effects, which can indicate the occurrence of crystallization, lead to the definition of the threshold temperatures, which in the 92Si composition case were the following: 650, 700, 750 and 800 °C. The 88Si based glass was TT at 600, 650, 700 and 800 ° C. [16;17]

The 92Si based glass was also subjected to thermoelectric treatments (TTE), which followed the same thermal profile of the TT. The 92Si based samples were therefore TTE at 650, 700 and 750 °C, for 4 hours. For each temperature, three different TTE were performed, differing in the amplitude value of the electric field applied: i) 100 kV/m, ii) 500 kV/m and iii) 1000 kV/m. These values were selected based on the thickness of the samples and the characteristics of the dc voltage source.

7. 92Si samples composition results

Figure 6 shows the macroscopic aspect of the 92Si samples, TT at the temperatures of 650, 700 and 750 °C. The based glass, completely transparent, becomes translucent for temperatures above 700 °C.

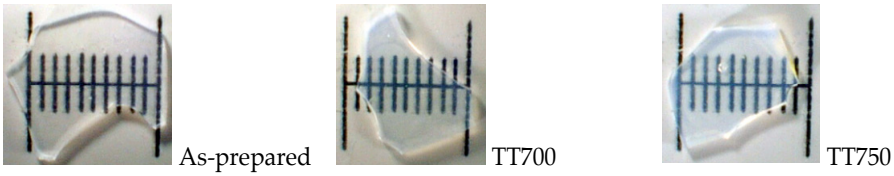

Figure 6. Photographs of the 92Si TT glasses (minor division = 0 1 mm).

The 92Si samples, TTE, were named as: 650A (sample TTE at 650 °C with an electric field of 100 kV/m), 650B (sample TTE 650 °C with an electric field of 500 kV/m) and 650C (TTE sample at 650 °C with an electric field of 1000 kV/m). The same designation was used in TTE samples at temperatures of 700 (700A, 700B ...) and 750 °C. In figure 7, photographs of all samples subjected to those treatments can be seen.

The samples 650A, 700A and 750A (samples TTE with a field amplitude of 100 kV/m) have a macroscopic aspect very similar to the sample 650B. With the increase of the TET temperature and applying 500 kV/m and 1000 kV/m, all samples become translucent.

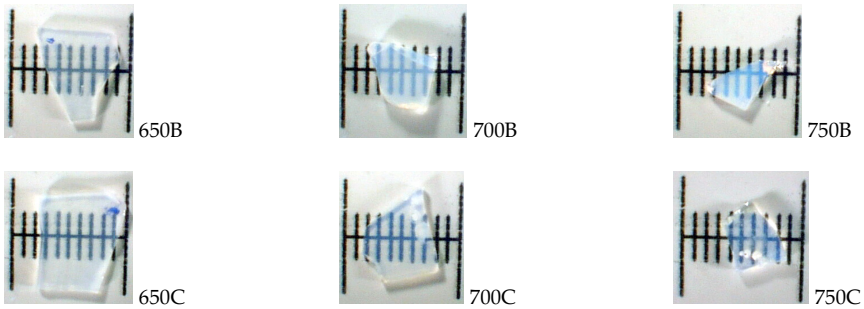

Figure 7. Photographs of the TTE samples at 650, 700 and 750 ºC, with the applied field of (B) 500 kV/m and (C) 1000 kV/m (minor scale division = 1mm).

Figure 8 shows the XRD patterns of the 92Si samples thermal treated without the presence of the external electrical field (TT). It can be observed for the samples TT at temperatures above 700 °C the presence of diffraction peaks associated with the $LiNbO_3$ crystalline phase. The sample TT at 800 °C also presents a second crystalline phase (SiO_2, quartz). The X-ray diffraction was performed at room temperature on a Phillips X'Pert system, where the X-ray production is performed on a Cu ampoule, operating at 40 kV and 30 mA, emitting the monochromatic Kα radiation (λ = 1,54056 Å - graphite monochromator). In this system the sweep is continuous, from 10.025 up to 89.975 º (2θ) with a speed of 1.5 degrees per minute and with a step of 0.02 º. The identification of the crystalline phases was based on the database provided by the JCPDS (Joint Committee on Powder Diffraction Standards). The figures 9 to 11 present the XRD spectra of the samples TET at 650, 700 and 750 ºC, respectively.

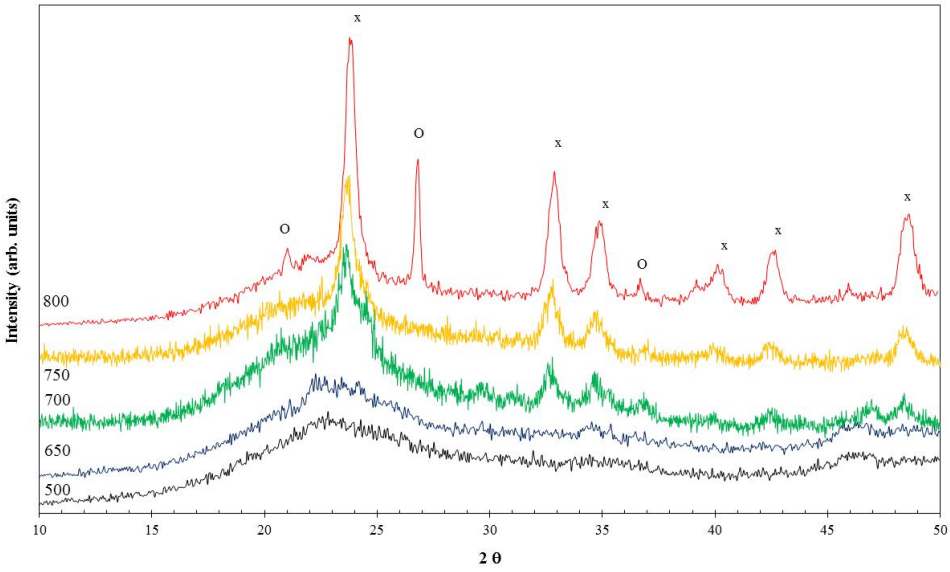

Figure 8. XRD of the 92Si samples TT at 650, 700, 750 and 800 ºC (x $LiNbO_3$; O SiO_2-quartzo).

The XRD spectra of the samples series treated at 650 °C (Fig. 9) shows that the increase in amplitude of the external electrical field favors the formation of the $LiNbO_3$ crystalline phase. In the sample series treated at the temperatures of 700 °C and 750 ºC (Figs. 10 and 11) it was detected the presence of $LiNbO_3$, SiO_2 (quartz) and $Li_2Si_2O_5$ crystalline phases. It is important to refer that the $Li_2Si_2O_5$ phase only appears in the samples thermo-electrically treated.

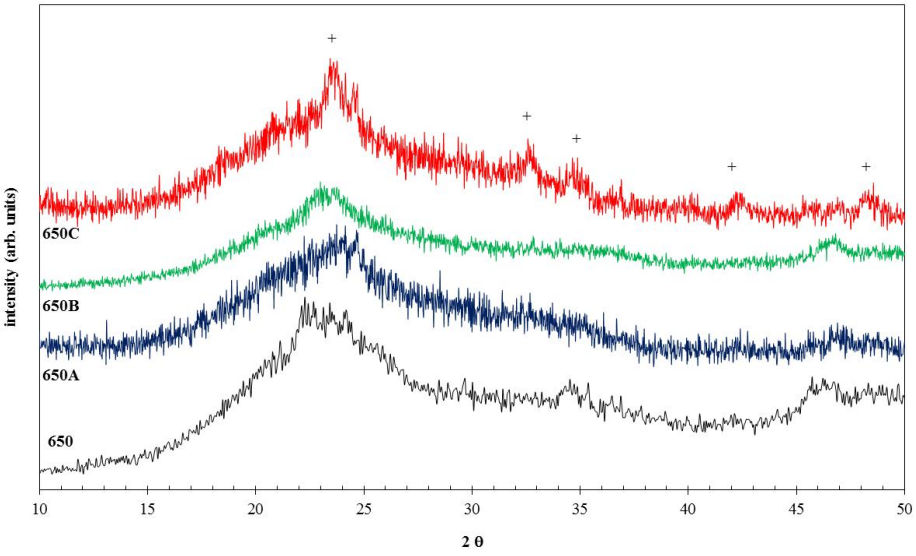

Figure 9. XRD spectra of the 92Si samples TET at 650ºC (+ $LiNbO_3$).

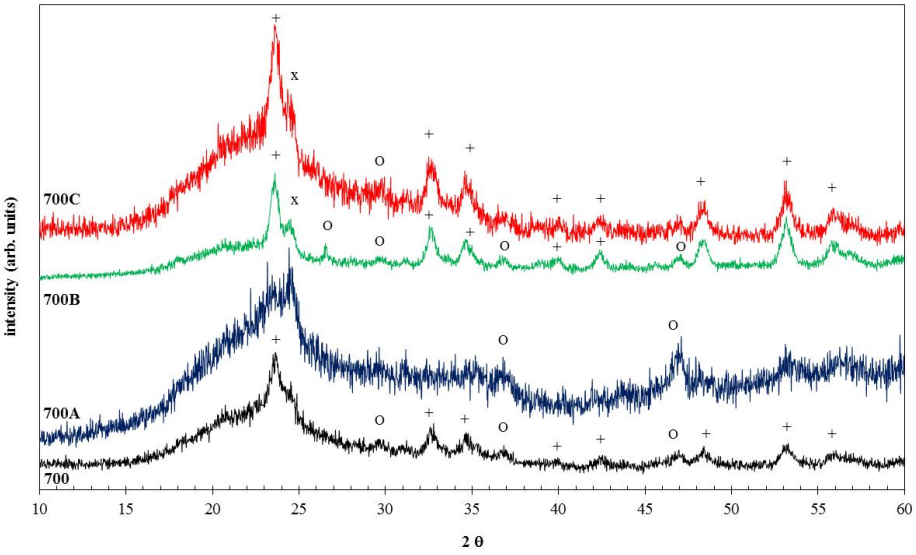

Figure 10. XRD spectra of the 92Si samples TET at 700ºC (+ $LiNbO_3$; O SiO_2 (quartz); x $Li_2Si_2O_5$).

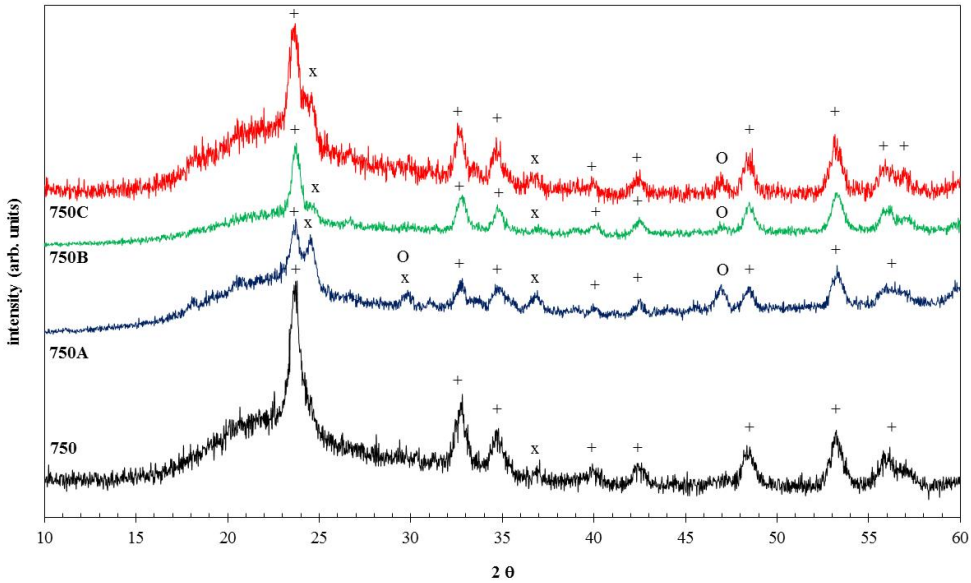

Figure 11. XRD spectra of the 92Si samples TET at 750^{0}C (+ $LiNbO_3$; O SiO_2 (quartz); x $Li_2Si_2O_5$).

Figures 12 to 15 show the Raman spectra of the free surface of the heat treated samples with or without external electrical field applied. It must be motes that no differences were detected between the spectra obtained on the free surface of the samples and fracture zones (bulk). This analysis was performed on a spectrometer T64000, Jobin Yvon SPEX using an argon laser operating at 514.5 nm. The Raman spectrum was obtained with a back-scattering geometry (back-scattering) between 100 and 2000 cm^{-1}. The amplitude of the lens used was of 50x which allows a laser spot diameter on the sample of about 5 mm.

In all Raman spectra (Figs. 12 to 15), the bands centered at 630, 590, 435, 375, 335, 330, 325, 280, 265, 240 and 155 cm^{-1} are associated to vibrations of the NbO_6 octahedrons [20;21;22]. The bands at 465, 415 and 130 cm^{-1} (sample 700C) are assigned to vibration of Si-O-Si bonds [23]. The broad band centered at 330 cm^{-1}, observed in the samples treated in the presence of an electric field of 1000 kV/m (samples C), seems to be due to the overlapping of the bands centered at 335 and 325 cm^{-1}. The band at 830 cm^{-1}, detected in the samples treated at 650 °C, with no external field applied, are attributed to the vibrations of the Nb-O-Si bonds [20;21;22;23;24].

In the following figures (Figs. 16) SEM micrographs of the free surface of the samples treated with and without the presence of an external electrical field are presented. The scanning electron microscopy was performed in a Hitachi S4100-1, on the surface and fracture of the samples covered with carbon.

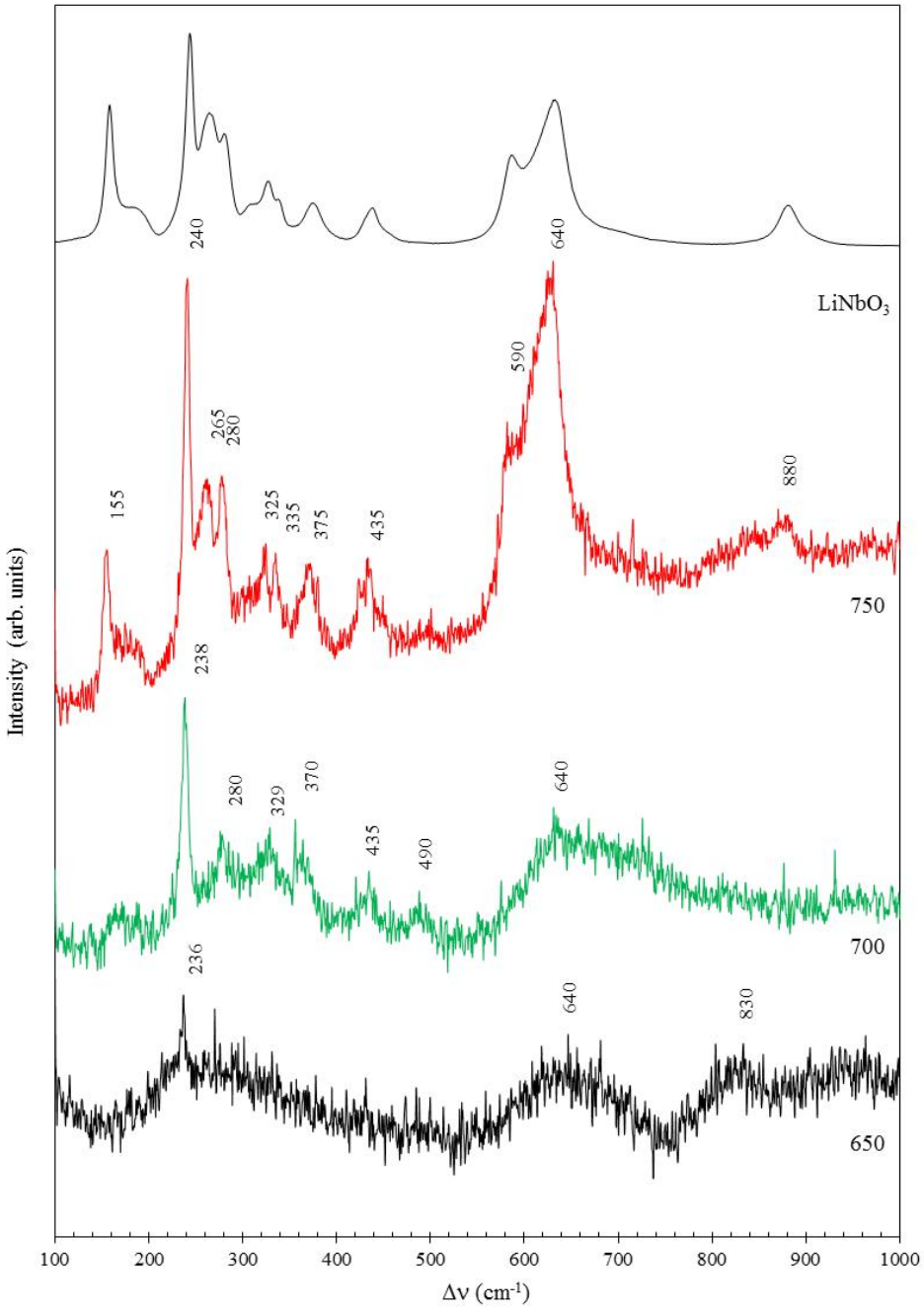

Figure 12. Raman spectra of the 92Si samples TT at 650, 700 and 750 ºC. The Raman spectrum of LiNbO3 crystalline powders is also presented.

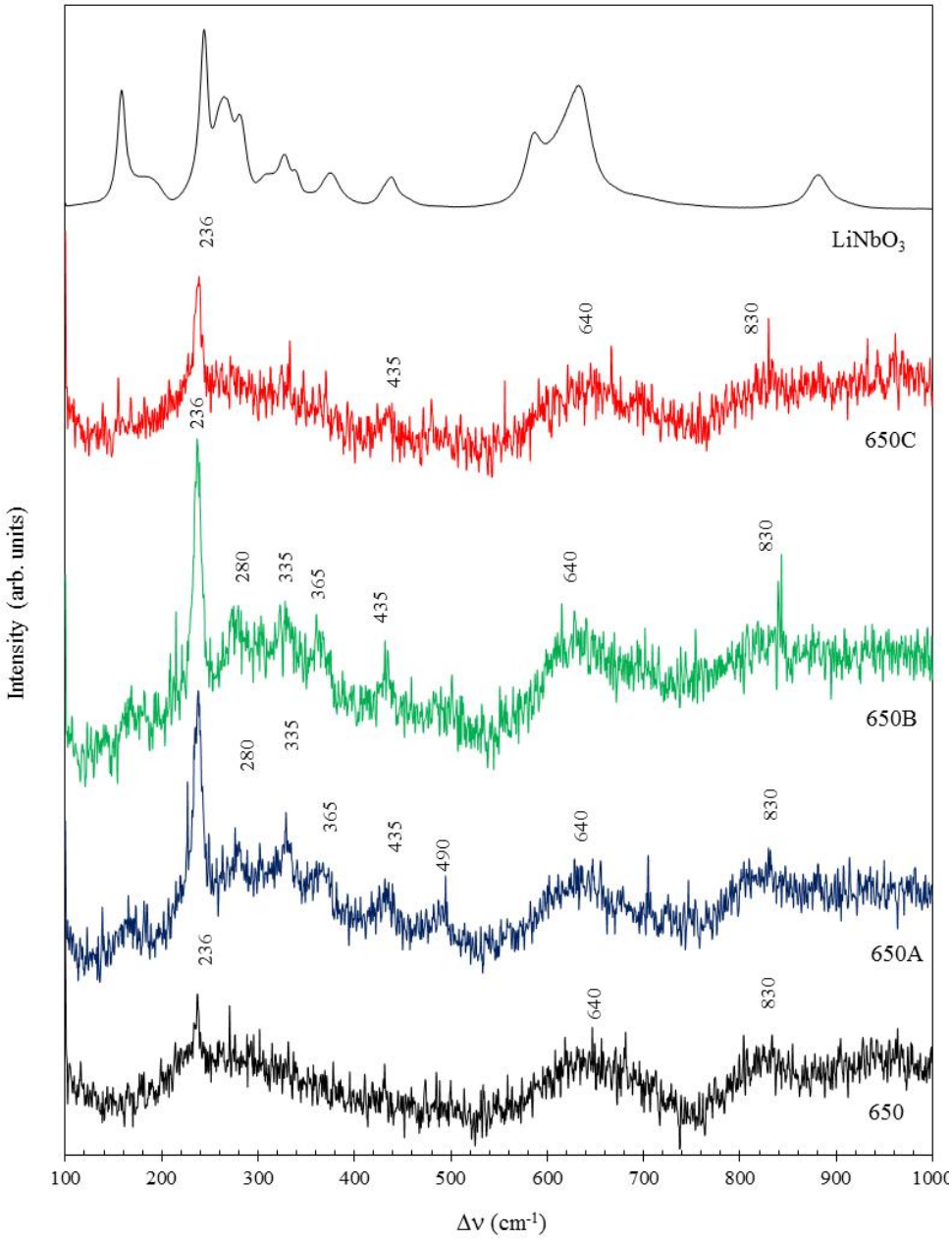

Figure 13. Raman spectra of the 92Si samples TET at 650 ºC. The Raman spectrum of $LiNbO_3$ crystalline powders is also presented.

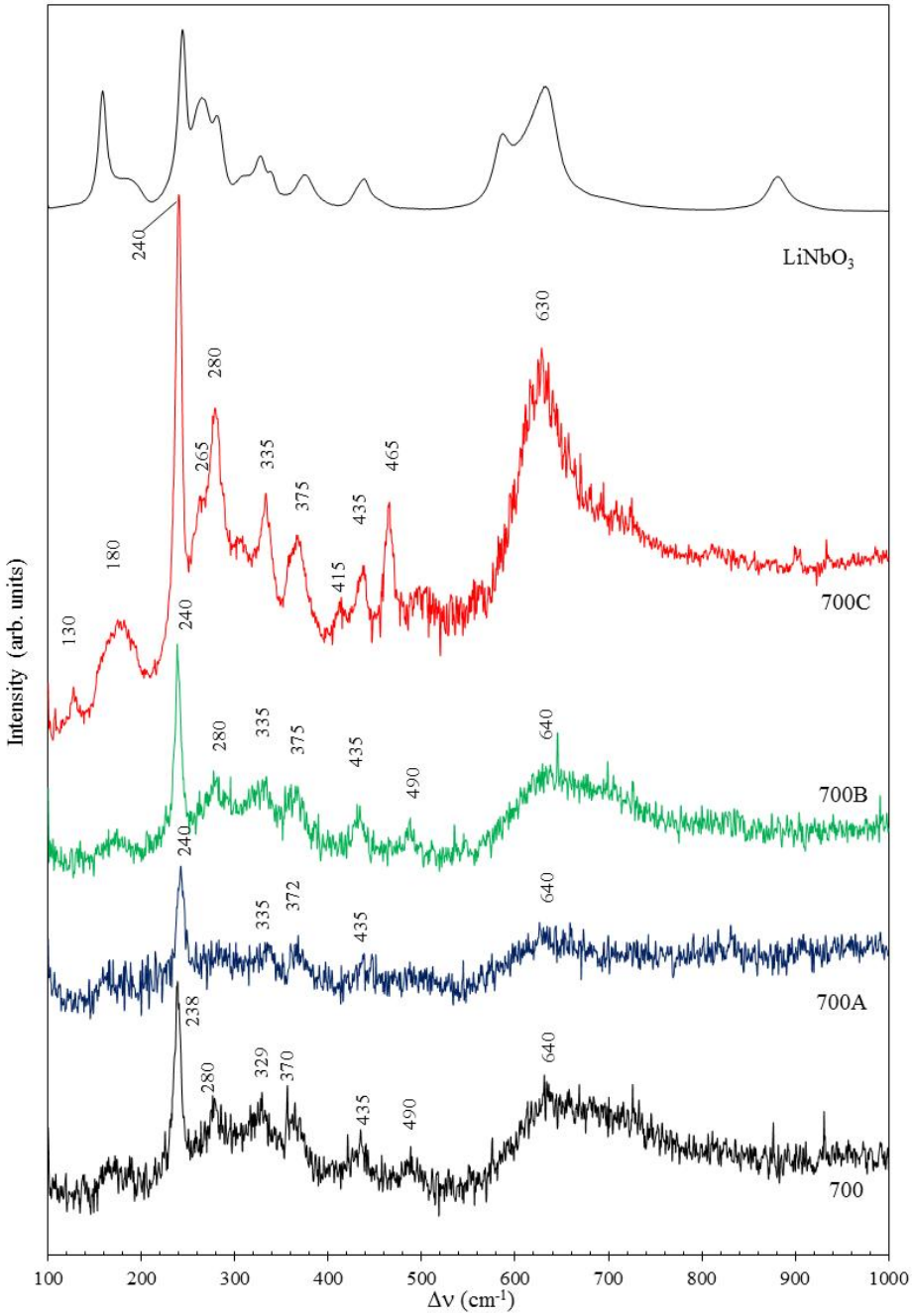

Figure 14. Raman spectra of the 92Si samples TET at 700 ºC. The Raman spectrum of $LiNbO_3$ crystalline powders is also presented.

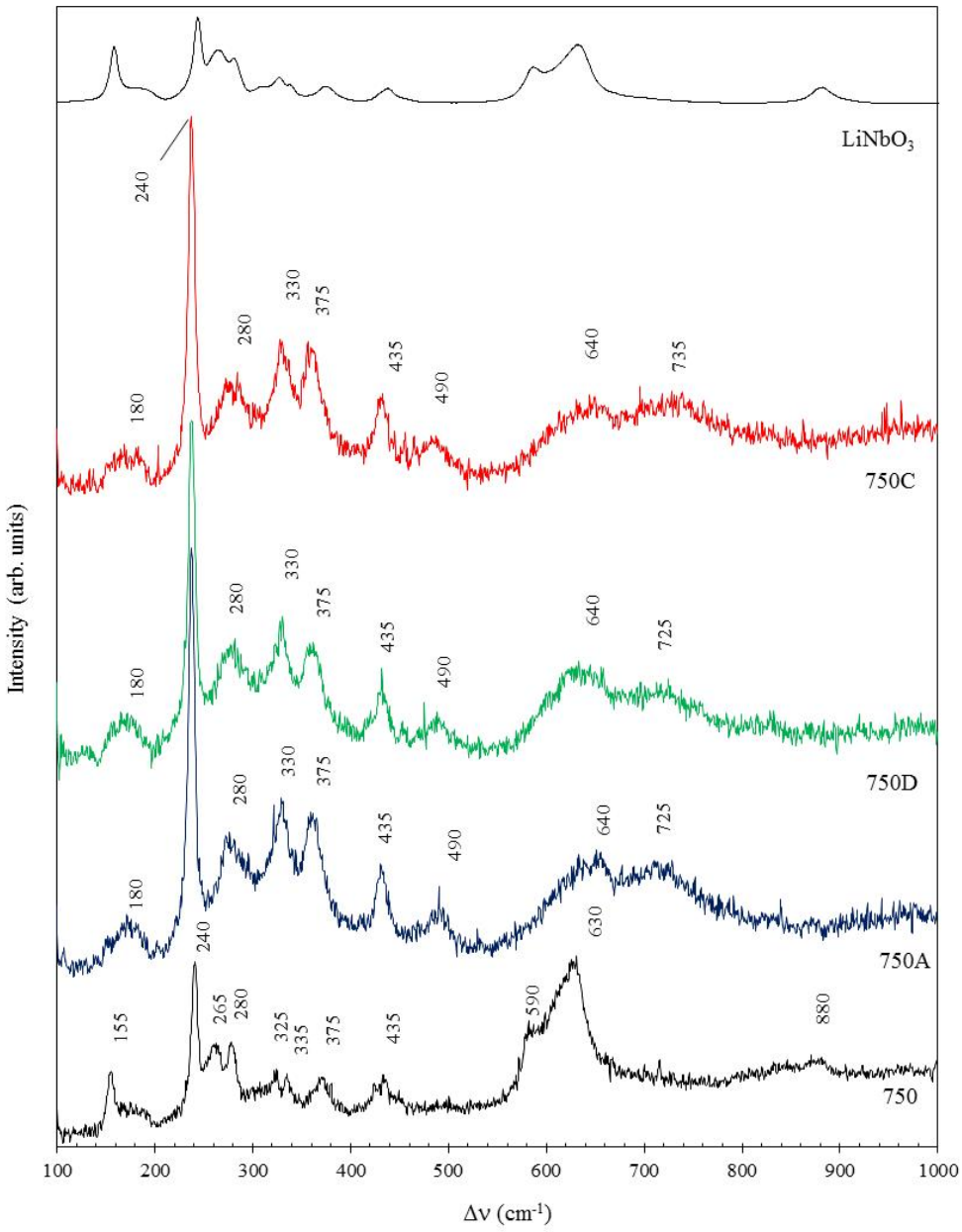

Figure 15. Raman spectra of the 92Si samples TET at 750 ºC. The Raman spectrum of $LiNbO_3$ crystalline powders is also presented.

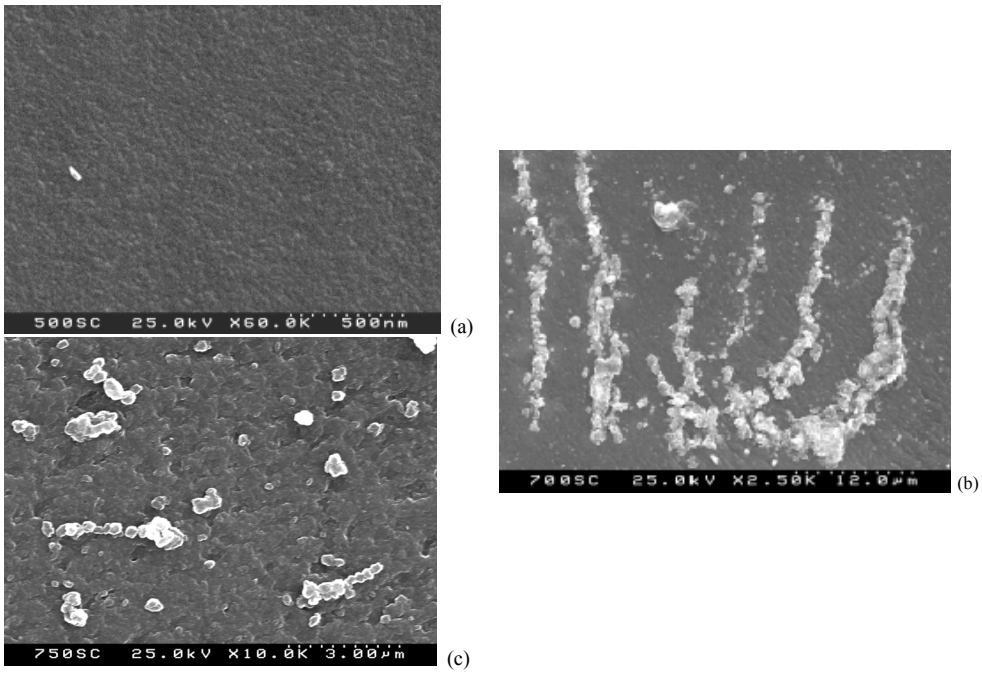

Figure 16. SEM micrographs of the 92Si samples: a) as-prepared; b) TT at 700 ºC; c) TT at 750 ºC.

It was observed in the SEM micrographs of the 92Si based glass (sample TT at 500 °C) the inexistence of particles. Increasing the treatment temperature an increase in the number of surface particles is induced. In the sample heat treated at 700 °C, without applying the external electric field (Fig. 16), particles showing a preferential growth direction were observed. On the surface of the sample TT at 750 °C (Fig. 16c), particle with a size of approximately 500 nm are observed and with a distribution similar to that observed in the sample TT at 700 °C. It must be notice that it was not detected in any sample of the 92Si series, the existence of particles in fracture zone (bulk). In the samples TET at 650 °C it was observed an increase in the size and number of the particles dispersed in the glass matrix, with the increase in amplitude of the applied field (Fig. 17).

In the sample 700A, the number of particles present on the surface, which during the TTE was in contact with the positive electrode, is greater than that the number observed on the opposite surface, but with similar sizes (~ 100nm). The sample 700B registered a particle size distribution similar to the one observed in the sample 700A, but with a larger size (~ 1 µm). Increasing the amplitude of the external electric field up to 1000 kV/m (sample 700C) it was observed the presence of particle aggregation in the two opposite surfaces of the sample. However, the number and size of those aggregates are larger in the surface that was in contact with the positive electrode. The growth of those aggregates seems to have a preferred direction.

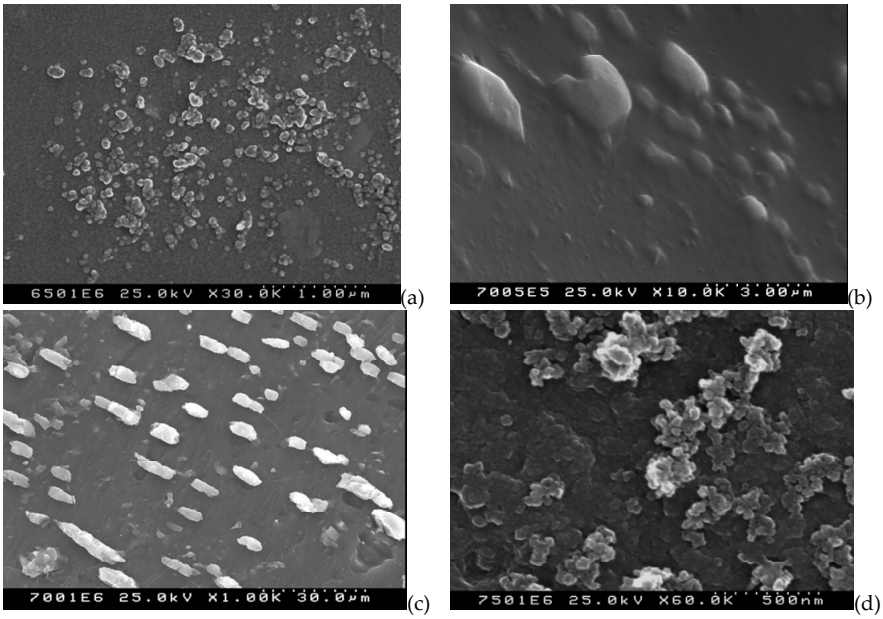

Figure 17. SEM micrographs of the samples 92Si TET: (a) 650C; (b) 700B; (c) 700C; (d) 750C.

Increasing the amplitude of the external electrical field, in the TET at 750 °C, it was observed an increasing in the number of particles but with a reduction in their size. Samples 750A and 750B have particles with an average size of 300 and 250 nm, respectively. The sample 750C presents particles with a maximum size of ~ 50 nm. These particles tend to aggregate themselves.

The dependence of the dc conductivity, in logarithm scale ($\ln(\sigma_{dc})$), with the temperature of measurement, for the samples TT at 650, 700 and 750 °C, with or without external electrical field applied, is shown in figures 18 to 20. All samples exhibit, for temperatures below 270 K, dc conductivity values (σ_{dc}) lower than 10^{-15} Sm^{-1}. The sample 750C shows the highest σdc value (2.63×10^{-9} Sm^{-1}), at the temperature of 370 K. With increasing the treatment temperature, the σ_{dc} measured at 300 K, decreases. These measurements also showed that the σ_{dc} is lower in samples treated with an electric field of 100 kV/m of amplitude (samples 650A, 700A and 750A) than in the samples treated without the presence of the external electrical field. In all sample series (650, 700 and 750), the increase of the amplitude of the electric field applied during the heat treatment induces an increase in σ_{dc} (Table 1).

The dependence of the σ_{dc} with the measurement temperature was adjusted by the Arrhenius equation [25;26;27] -

$$\sigma_{dc} = \sigma_0 e^{\left(-\frac{E_A}{kT}\right)}$$

This adjustment presented graphically in figures 14 to 16 by the lines, allowed the calculation of the dc activation energy ($E_{a(dc)}$ – table 1). It is observed, in all samples, the existence of at least two regions with different activation energies. The first (A), between 270 and 300 K, and the second (B), between 345 and 370 K. The activation energy associated with the conduction mechanism detected at higher temperatures ($E_{a(dc)}$ (B), Table 1) decreases with the increase of the amplitude of the applied electric field, for the sample series treated at 700 and 750 °C. It is observed, with the exception of the sample 700A, that the activation energy of the process A (at lowest temperatures) is always lower than the $E_{a(dc)}$ of the process B.

Sample	σ_{dc} x 10^{-14} ($\Omega^{-1}m^{-1}$)	$E_{a(dc)}$ (A) (kJ/mol)	$E_{a(dc)}$ (B) (kJ/mol)
650	128,48 ± 5,15	24,64 ± 1,19	79,98 ± 1,12
650A	2,04 ± 0,06	27,91 ± 1,09	62,66 ± 2,66
650B	3,03 ± 0,09	27,94 ± 1,40	77,56 ± 0,95
650C	36,46 ± 1,46	48,83 ± 0,72	64,22 ± 1,41
700	13,21 ± 0,55	46,47 ± 1,92	72,98 ± 0,78
700A	4,96 ± 0,21	32,63 ± 3,00	71,38 ± 3,97
700B	8,64 ± 0,29	66,35 ± 1,02	66,79 ± 0,83
700C	15,18 ± 0,47	100,18 ± 3,31	57,15 ± 0,99
750	12,39 ± 0,43	31,48 ± 0,29	51,02 ± 1,55
750A	6,09 ± 0,35	31,63 ± 0,68	82,08 ± 3,19
750B	21,71 ± 1,06	7,71 ± 2,08	79,26 ± 0,82
750C	393,87 ± 12,91	24,47 ± 2,59	62,88 ± 1,22

Table 1. dc conductivity (σ_{dc}), at 300 K, dc activation energy ($E_{a(dc)}$) for the: A - low temperature region (230-300 K); B – high temperature region (310-370 K).

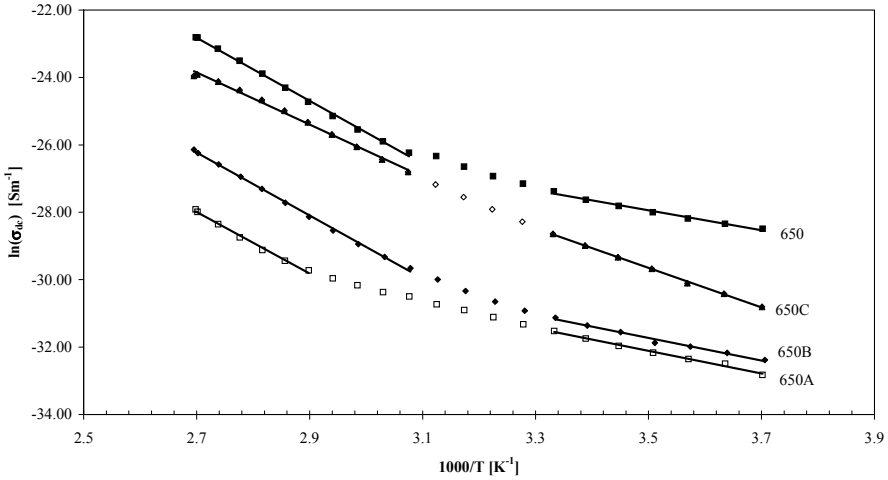

Figure 18. The dc conductivity (σ_{dc} , in logarithm scale) in function of 1000/T, for the 92Si samples treated at 650 ºC.

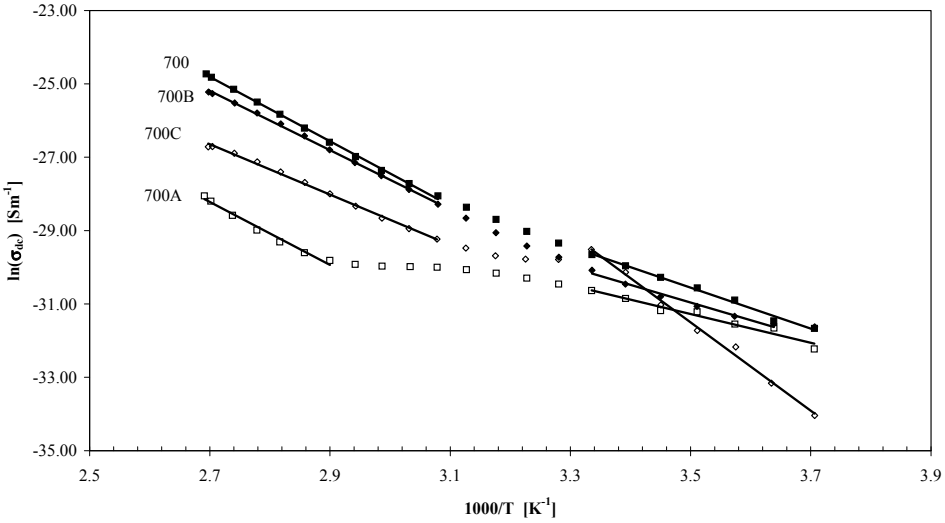

Figure 19. The dc conductivity (σ_{dc}, in logarithm scale) in function of 1000/T, for the 92Si samples treated at 700 ºC.

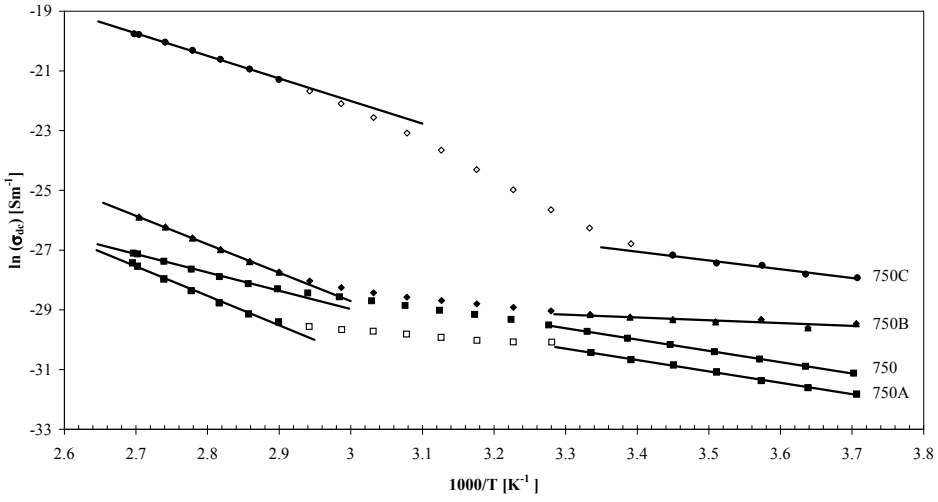

Figure 20. The dc conductivity (σ_{dc}, in logarithm scale) in function of 1000/T, for the 92Si samples treated at 700 ºC.

Figures 21 to 23 show the frequency dependence of the imaginary part of the impedance (Z´´) for the sample series treated at 650, 700 and 750 °C, respectively. It was observed, for

the samples series treated at 650 and 700 °C, that Z'' decreases with the increase of frequency. In the frequency range used, the impedance (Z*), the admittance (Y*), the permittivity (ε*) and the dielectric modulus (M*) formalisms did not revealed the existence of dielectric relaxation(s). It must be noted that, for frequencies below 100 Hz, there is a high dispersion of the Z´´ values, which is associated with the sensitivity of the measuring apparatus, in this frequency range.

An adjustment of the Z* spectrum was carried out using a complex non-linear least squared deviations method (CNLLS) associated with the electrical equivalent circuit model formed by the parallel between a resistor (R) and a constant phase element (CPE). This constant phase element is characterized by keeping constant the angle of the impedance as a function of frequency, i.e. the ratio between the real and imaginary part of the impedance is constant across the all frequency range. The impedance of this intuitive element (Z_{CPE}) can be represented by

$$Z_{CPE} = \frac{1}{Q_0 (j\omega)^n}$$

where Q_0 and n are frequency independent parameters, but usually are temperature dependent. The parameter n varies between 0 and 1, when n = 1 the CPE is reduced to a capacitance element and when n =0 to a resistive element [18].The lines ("small dots") in the figures 21 to 23 represent the result of this adjustment. The values obtained for the parameters of the equivalent electric circuit are in table 2.

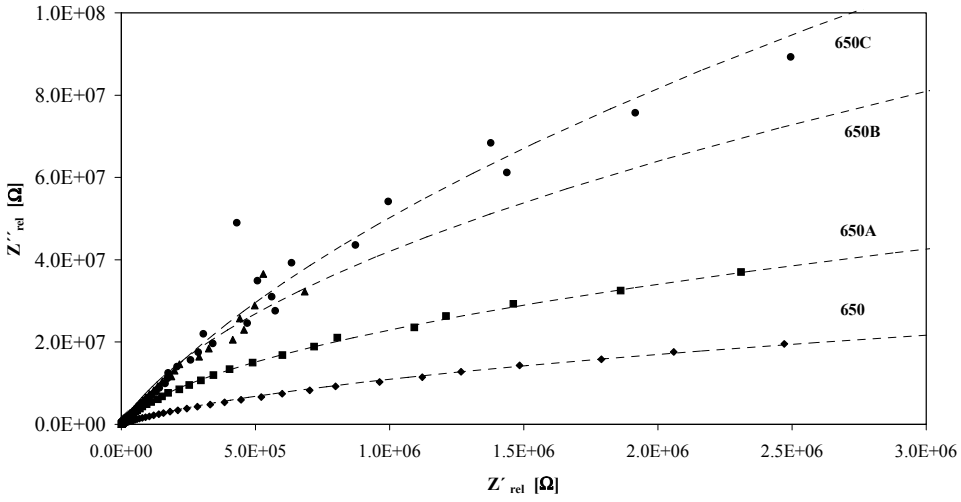

Figure 21. Z´´ versus Z´, for the 92Si samples treated at 650 ºC.

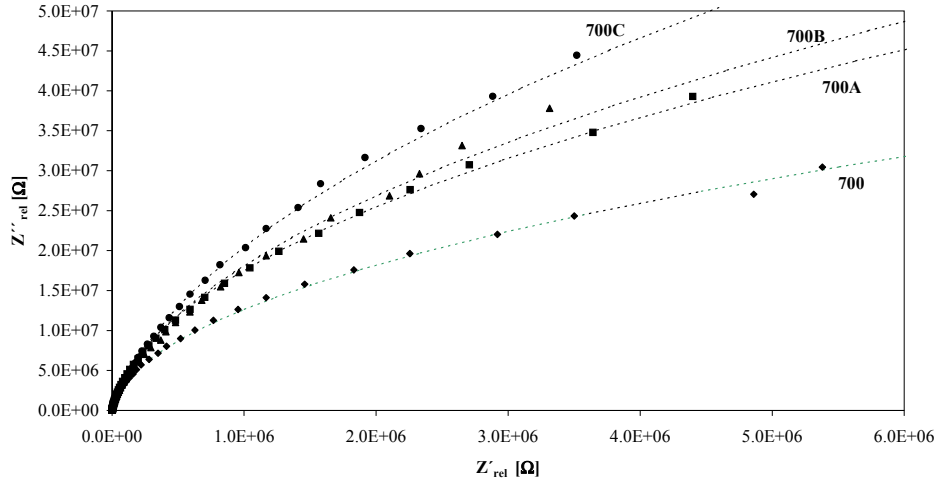

Figure 22. Z´´ versus Z´, for the 92Si samples treated at 700 ºC.

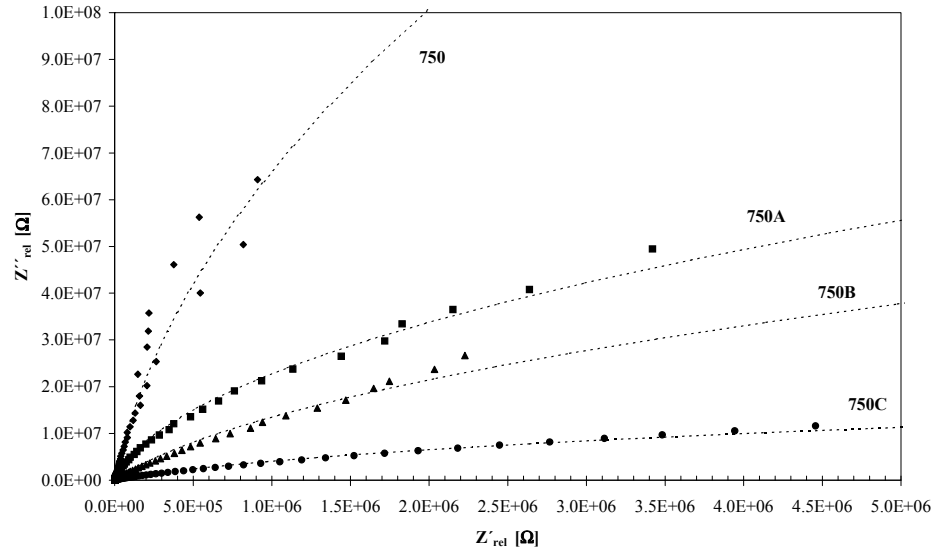

Figure 23. Z´´ versus Z´, for the 92Si samples treated at 750 ºC.

From the results obtained through the CNLLS fitting process, it is verified that the R parameter, of the samples treated at 650 and 700 °C increases, with the increase of the amplitude of the external electric field. In the sample series treated at 750 °C this parameter has the opposite behavior, i.e., it decreases with the increase of the applied electric field amplitude. However, it should be referred that the sample treated at 750 °C, but without the presence of an external electric field, shows the lowest value of R and the sample 750C (TTE

with a field of 1000 kV/m) the largest value of R for all samples. The behavior of the Q_0 parameter, in function of the thermal treatment conditions, is opposite to the observed for parameter R. In all samples, the value of the parameter n is very close to 1. Based on these calculated values a relaxation time, which represents the time average of the relaxation time distribution, was calculated ($\tau_Z = 1/\omega_{Z''_{max}}$) and the value of the capacity nearest of the CPE element value (Table 2). Evaluating the behavior of the parameter τ_Z (Table 2), with the increase of the electric field amplitude, it is verified that τ_Z increases with the increase of that amplitude in the sample series treated at 650 and 700 °C. In the samples treated at 750 °C, the increase of the amplitude of the external electrical field, induces an opposite behavior, i.e., a decrease of τ_Z.

Sample	ε´	tan δ (x10^{-2})	R (x10^{8}) [Ω]	Qo (x10^{-11}) [Ω^{-1}m^{-2}s^{n}]	n (x10^{-1})	τ_Z (x10^{-3}) [s]	C_{CPE} (x10^{-11}) [F]
650	5,21 ± 0,18	6,13 ± 0,34	2,34	6,01	9,72	1,96	5,76
650[a]	4,66 ± 0,12	1,81 ± 0,07	7,41	4,47	9,92	5,13	4,46
650B	4,82 ± 0,14	1,29 ± 0,06	23,90	4,54	9,94	20,94	4,54
650C	2,03 ± 0,07	1,61 ± 0,12	68,51	1,94	9,92	20,67	1,94
700	5,57 ± 0,20	2,79 ± 0,16	1,85	5,25	9,93	1,50	5,24
700[a]	4,41 ± 0,16	2,39 ± 0,14	3,75	4,17	9,94	2,42	4,16
700B	4,50 ± 0,14	2,68 ± 0,13	4,59	4,41	9,90	3,10	4,38
700C	3,82 ± 0,11	2,92 ± 0,13	7,19	3,79	9,87	4,14	3,77
750	2,79 ± 0,09	8,40 ± 0,05	7,45	2,56	9,96	29,47	2,56
750[a]	3,68 ± 0,19	2,03 ± 0,17	7,26	3,52	9,92	3,95	3,51
750B	6,07 ± 0,27	5,86 ± 0,40	4,26	6,91	9,73	4,26	6,69
750C	9,44 ± 0,28	21,20± 0,98	0,47	20,80	9,01	0,95	13,62

Table 2. Dielectric constant (ε´) and dielectric loss (tan δ), at 1kHz and 300 K, parameters of the equivalent electric circuit (R, Q_0 and n), relaxation time (τ_Z) and the C_{CPE} capacitor.

The dependence of the dielectric constant (ε') with the frequency, at the temperature of 300 K, for the sample series of 650, 700 and 750 is represented in figures 24 to 26, respectively. It is observed that the value of ε' decreases with the increase of the frequency. Table 2 shows the values of ε', measured at 300 K and 1 kHz, for all samples. It can be verified that the increase of the amplitude of the external electrical field, for the samples treated at 650 and 700 °C, promotes a decrease of ε'. In the samples series treated at 750 °C, ε' increases from 2.8 to 9.4, with the increase of the amplitude of the applied external electric field. The C_{CPE} capacitance behavior (Table 2), with the increase of the amplitude of the external electrical field, is similar to the one observed on the ε'. Table 2 contains also the values of the dielectric loss factor (tan δ = ε''/ε'), at room temperature (300 K) and at the frequency of 1 kHz.

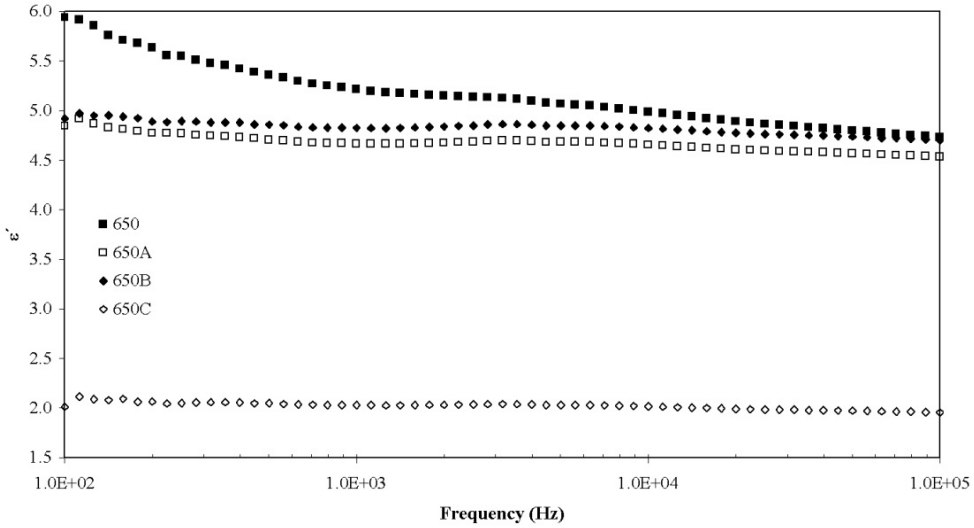

Figure 24. ε´ versus frequency, at 300 K, for the 92Si samples treated at 650 ºC.

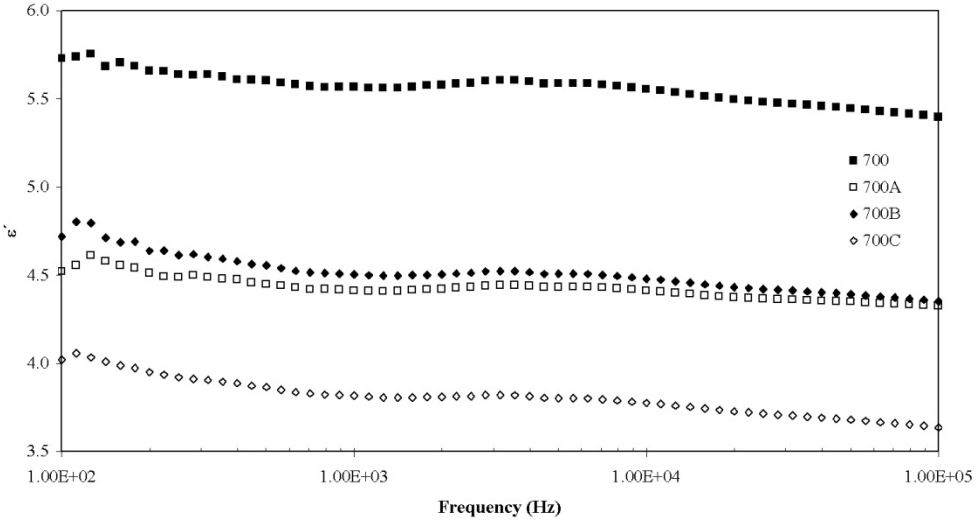

Figure 25. ε´ versus frequency, at 300 K, for the 92Si samples treated at 700 ºC.

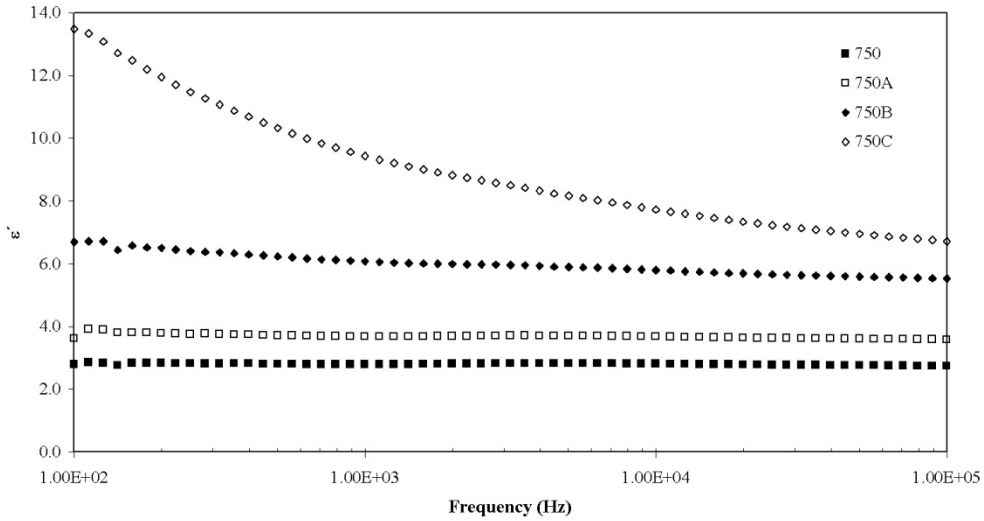

Figure 26. ε´ versus frequency, at 300 K, for the 92Si samples treated at 750 ºC.

8. 88Si samples composition results

Figure 27 shows the macroscopic aspect of the 88Si sample composition, TT at 500, 600, 650, 700 and 800 ºC, during 4 hours. It can be seen that the as-prepared glass (TT at 500 ºC) is translucent and for TT above 700 ºC it becomes opaque.

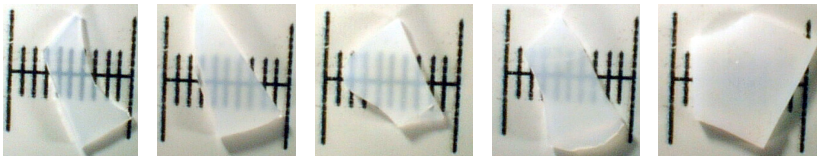

Figure 27. Photographs of the 88 Si samples TT at temperatures between 500 and 800 ºC (the minor scale division = 1mm).

Figure 28 shows the XRD patterns of the samples TT. This spectrum shows the presence of $LiNbO_3$ crystalline phases and cristobalite (SiO_2), in the samples treated at temperatures above 650 °C. With the increase of the TT temperature up to 700 °C it was detected also the lithium silicate ($Li_2Si_2O_5$) crystalline phase. In order to confirm the indexing of some diffraction peaks observed in the sample TT at 800 °C, the XRD was carried out in a new sample, TT at 800 °C but during 8h (sample 800-8h). Analyzing the pattern of this sample it is suggested the presence, in the samples treated at 800 °C, of the Li_3NbO_4 crystalline phase.

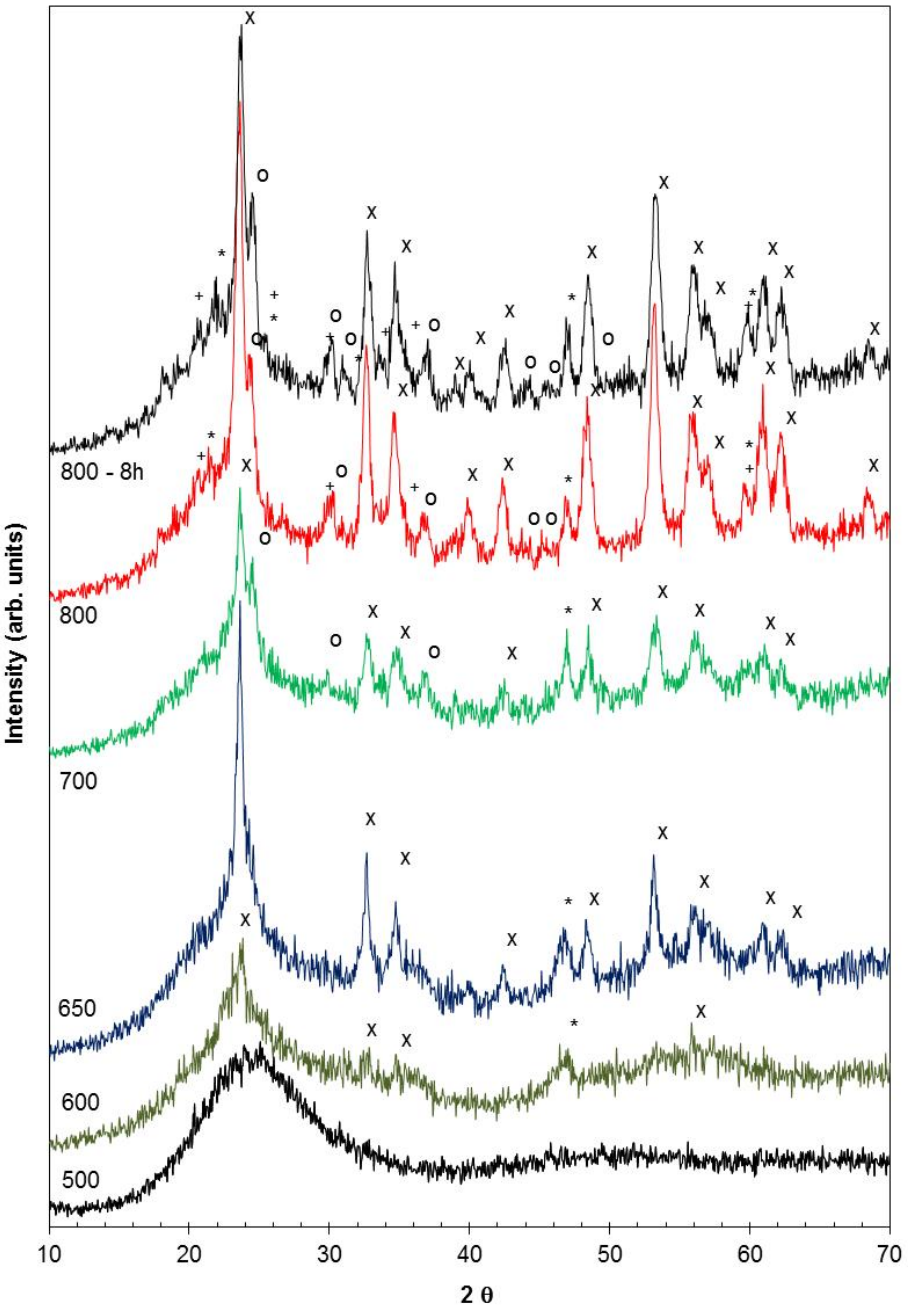

Figure 28. XRD spectra of the 88Si samples TT at temperatures between 500 and 800 ºC (x $LiNbO_3$; O $Li_2Si_2O_5$; * SiO_2 (cristobalite); + Li_3NbO_4).

In figure 29 it is shown the Raman spectra of the surface of all 88Si TT samples. The Raman spectrum of the samples treated at temperatures below 600 °C shows the presence of broad bands centered at ~ 680 and ~ 280 cm^{-1}. With the increase of the thermal treatment temperature, less wide bands but with higher intensity are detected. The bands centered at 630-680 and 240 cm^{-1} observed in samples TT at 500, 600 and 650 °C are due to vibrations of NbO_6 octahedrons [16;17]. The bands at 440, 360, 334 and 280 cm^{-1}, detected in the sample TT at 800 °C, are assigned to the vibration of NbO6 octahedrons, which are associated with the $LiNbO_3$ crystal structure [16;17]. It must be noted the non-detection of Raman bands associated with vibrations of the type Si-O-Si or Nb-O-Si. The non-detection of vibrations associated to Nb-Si-O bonds, which according to Lipovski et al. [24] should be present between 800 and 850 cm^{-1}, suggests that the niobium ions are introduced into the glass matrix only as network modifier.

Micrographs of the sample surface of the 88Si samples TT at 500ºC, 600, 650, 700 and 800 °C are shown in figure 30. The SEM micrographs show, in the surface of the sample heat-treated at 600 °C, particles (Fig. 30b). The size of those particles, also observed in samples TT at 700 and 800 ºC is similar (150-200 nm). However, increasing the temperature of TT leads to an increase in the number of particles. The sample TT at 650 °C has a particle size of around 2 μm (Fig. 30c). The micrograph of this sample also present particle agglomerates (Fig. 30d), not detected in any other sample.

The dependence of the dc conductivity with the temperature of measurement, for all TT samples, is shown in figure 31. The Arrhenius model was used to adjust the $\ln(\sigma_{dc})$ with the inverse of the measurement temperature, allowing the calculation of the activation energy ($E_{a(dc)}$) through the Arrhenius equation. From figure 31 it is verified the existence of two temperature zones, with different activation energies. The first zone (A) is between 230 and 300 K and second (B) is between 310 and 370 K. The as-prepared sample (TT at 500 °C) presents, for measuring temperatures above 300 K, a behavior that is non-adjustable through the Arrhenius equation. The calculated values of $E_{a(dc)}$ are shown in Table 3.

The ac conductivity (σ_{ac}), measured at 300 K and 1 kHz, decreases with the increase of the TT temperature (Table 3). The activation energy, $E_{a(ac)}$, was calculated using the Arrhenius formalism. The lines in figure 31 represent the result of that calculation and the obtained values are in Table 3.

Figures 34 to 41 show the dependence of Z'' with the frequency, at various measurement temperatures, for all TT samples. It was observed the existence of two dielectric relaxation mechanisms. The first, in the low frequency region (< 100 Hz) and the second in the high frequency region (> 1 kHz). For frequencies below 1 Hz, a high dispersion of the Z* values is observed and assigned to the sensitivity of the measuring instrument in this low frequency region. The impedance spectra were adjusted to the electrical equivalent circuit model, shown in figure 33, using the CNLLS algorithm. Thus, in the spectra shown in figures 34 to 41, the lines represent the adjustment obtained with this fitting process. It is observed that with the increase of the temperature of measurement, there is a tendency for a better definition of the relaxation curves. Thus, and for the lower measuring temperatures it was found that the adjustment process diverged, not been possible to fit the experimental data with this theoretical model.

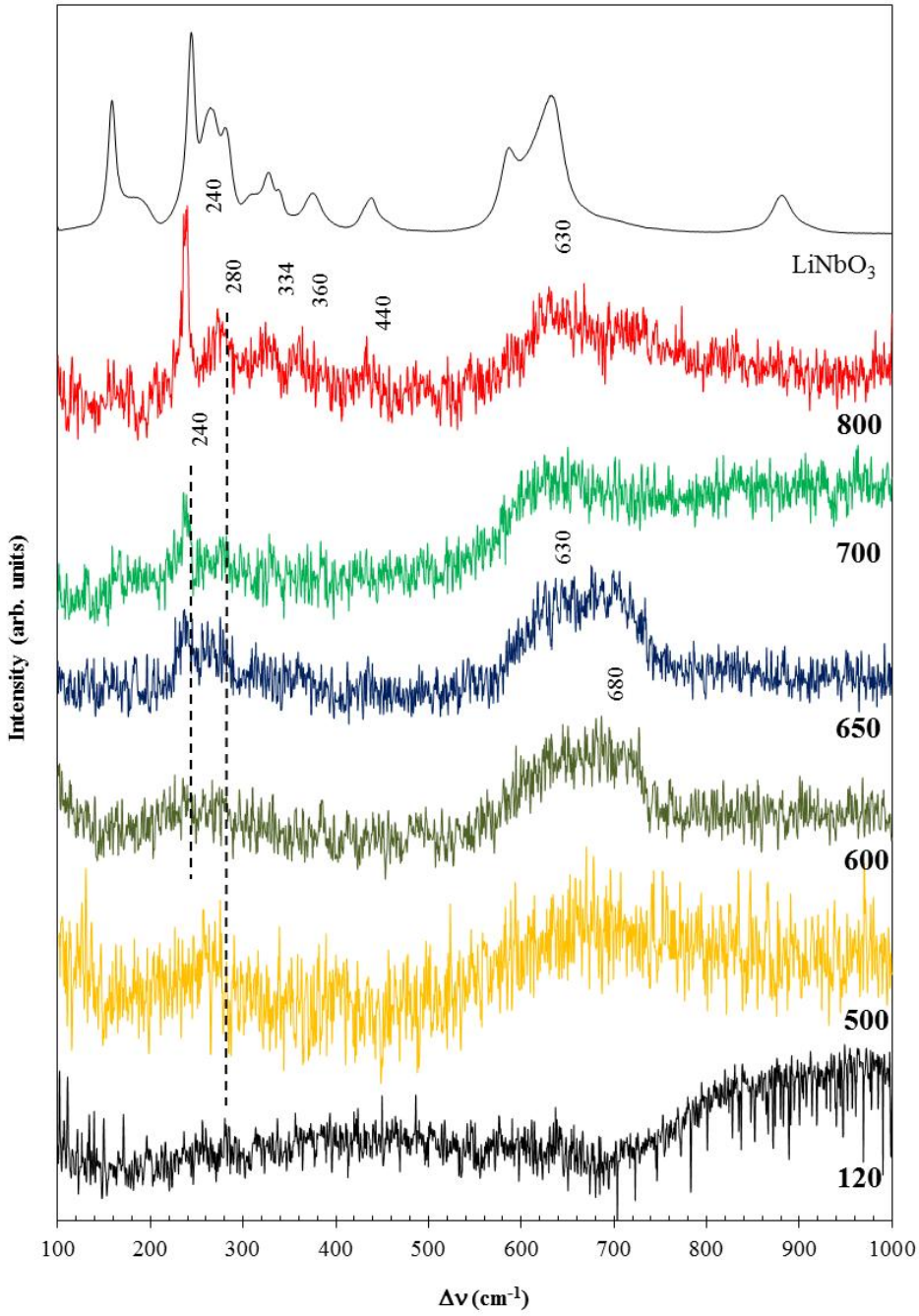

Figure 29. Raman spectra of the 88Si samples TT at 120, 500, 600, 650, 700 and 800 ºC.

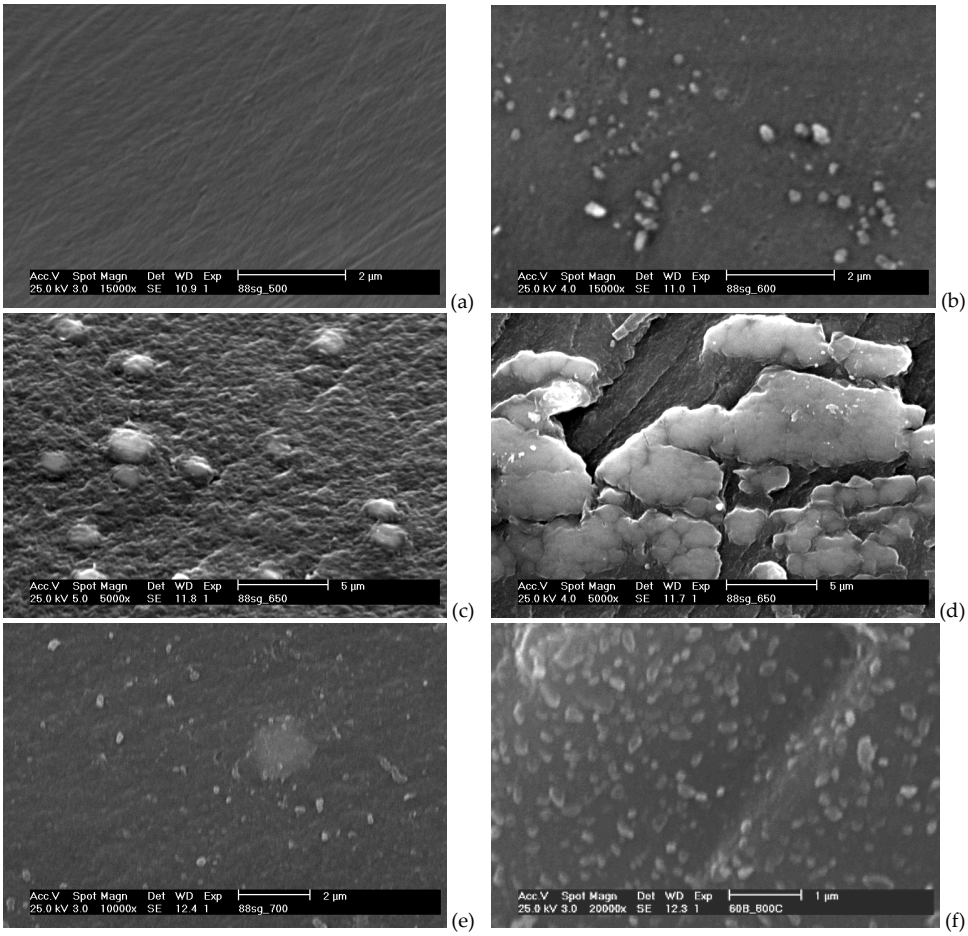

Figure 30. SEM micrographs of the 88Si samples: a) as-prepared (TT at 500 ºC); b) TT600; c) TT650; d) TT650; e) TT700; f) TT800.

Sample	σ_{dc} (x10^{-8}) [$\Omega^{-1}m^{-1}$]	$E_{a(dc)}$ (A) [kJ/mol]	$E_{a(dc)}$ (B) [kJ/mol]	σ_{ac} (x10^{-6}) [$\Omega^{-1}m^{-1}$]	$E_{a(ac)}$ [kJ/mol]
500	379,70 ± 9,86	50,95 ± 1,78	--	20,10 ± 0,02	45,79 ± 0,53
600	163,71 ± 2,41	57,66 ± 1,03	31,66 ± 1,71	15,02 ± 0,62	31,71 ± 0,31
650	55,42 ± 0,74	66,24 ± 0,40	44,00 ± 0,94	2,49 ± 0,09	52,17 ± 2,27
700	120,82 ± 1,66	64,35 ± 0,43	32,76 ± 0,77	2,80 ± 0,12	45,60 ± 2,70
800	3,47 ± 0,05	61,02 ± 0,89	49,96 ± 0,72	0,60 ± 0,02	43,83 ± 2,33

Table 3. dc conductivity (σ_{dc}), at 300 K, dc activation energy ($E_{a(dc)}$) for the: A - low temperature region (230-300 K); B – high temperature region (310-370 K).

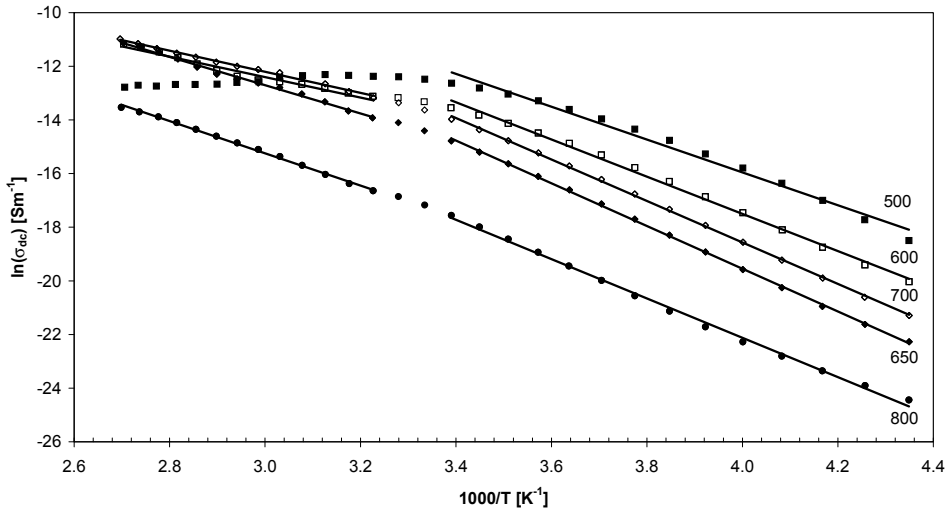

Figure 31. ln(σ_{dc}) versus 1000/T for all 88Si samples TT between 500 and 800 ºC.

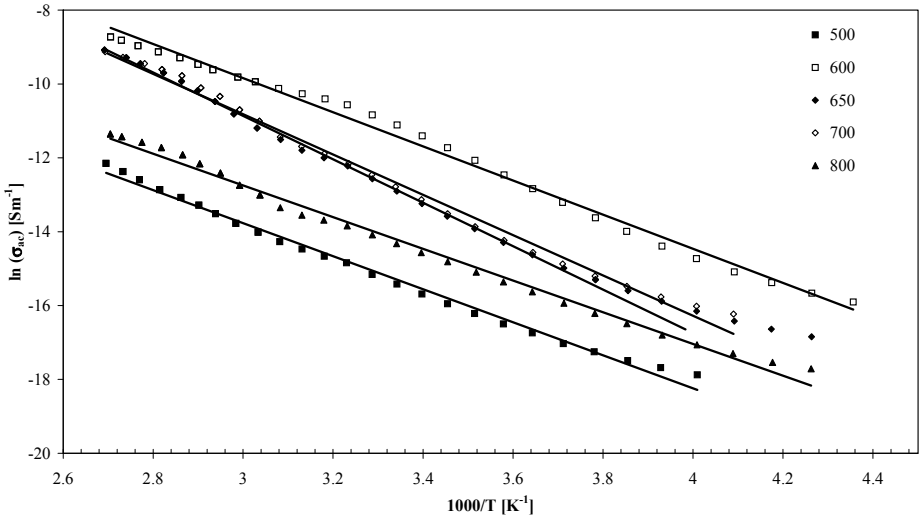

Figure 32. ln(σ_{ac}) versus 1000/T for the samples 88Si TT between 500 and 800 ºC.

Table 4 presents the parameter values of the electrical equivalent circuit for all analyzed samples. Note that the value of the parameter R_0, representing the value of Z' when $\omega \rightarrow \infty$ was considered equal to 0 Ω. The parameters R_1 and CPE_1 (CPE represents a constant phase element [18]) are associated with the dielectric relaxation mechanism found at low frequencies (< 100 Hz) and the parameters R_2 and CPE_2 with the relaxation mechanism detected in the high frequency region.

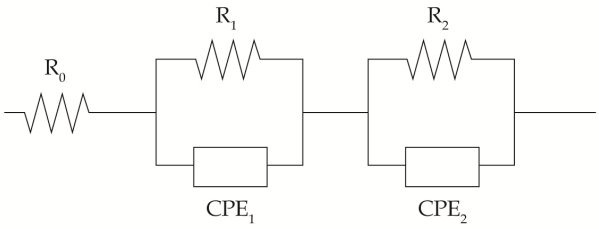

Figure 33. Equivalent electric circuit model used to adjust the impedance data of the 88Si samples ([$R_0(R_1CPE_1)(R_2CPE_2)$]).

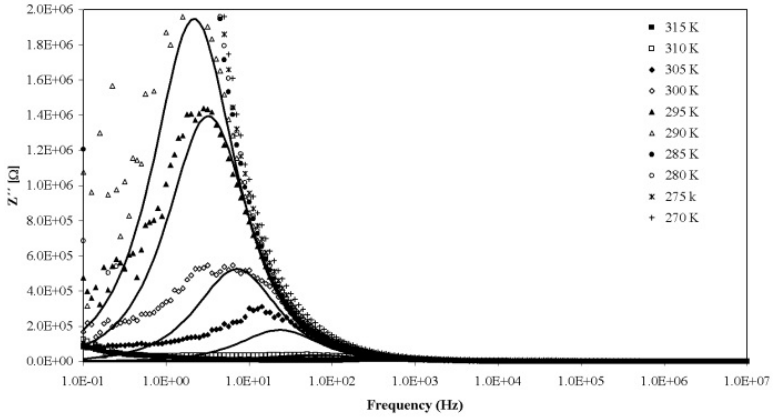

Figure 34. Z´´ versus frequency for the 88Si sample TT at 600 ºC (low frequency region). The lines represent the theoretical adjust.

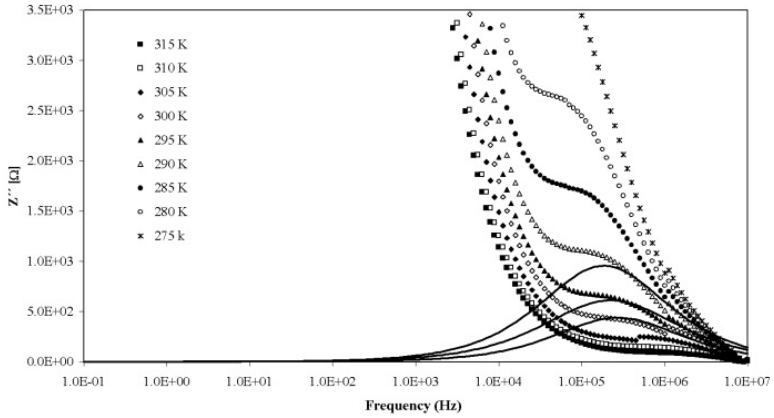

Figure 35. Z´´ versus frequency for the 88Si sample TT at 600 ºC (high frequency region). The lines represent the theoretical adjust.

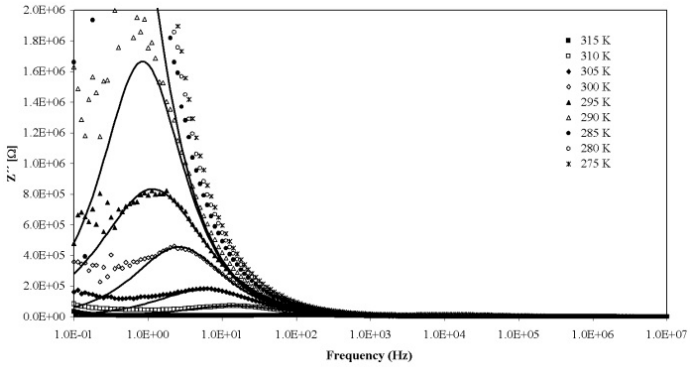

Figure 36. Z'' versus frequency for the 88Si sample TT at 650 ºC (low frequency region). The lines represent the theoretical adjust.

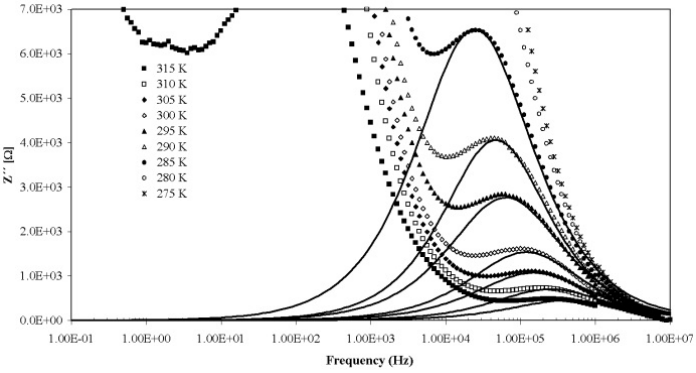

Figure 37. Z'' versus frequency for the 88Si sample TT at 650 ºC (high frequency region). The lines represent the theoretical adjust.

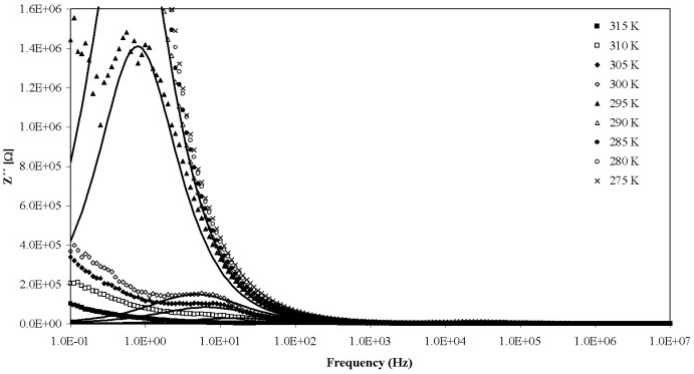

Figure 38. Z'' versus frequency for the 88Si sample TT at 700 ºC (low frequency region). The lines represent the theoretical adjust.

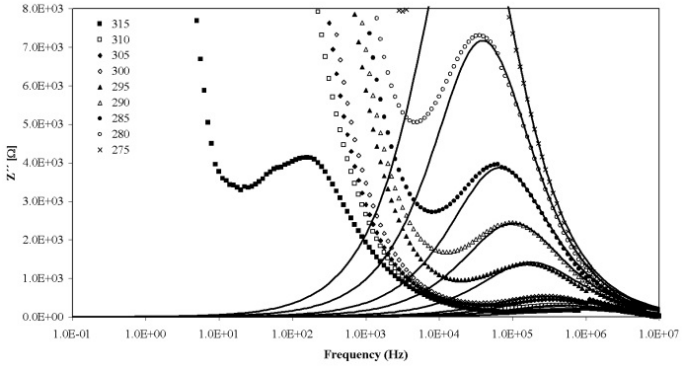

Figure 39. Z´´ versus frequency for the 88Si sample TT at 700 ºC (high frequency region). The lines represent the theoretical adjust.

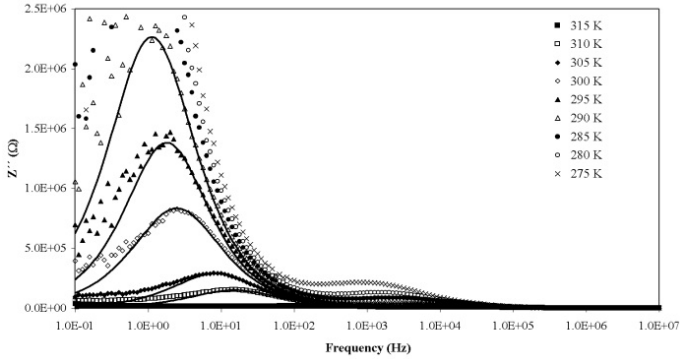

Figure 40. Z´´ versus frequency for the 88Si sample TT at 800 ºC (low frequency region). The lines represent the theoretical adjust.

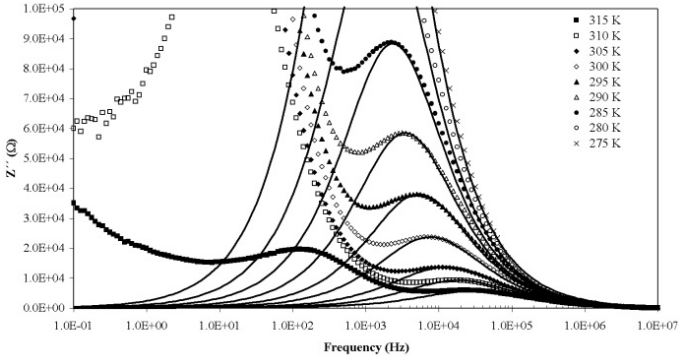

Figure 41. Z´´ versus frequency for the 88Si sample TT at 800 ºC (high frequency region). The lines represent the theoretical adjust.

Sample	Temp. (K)	R_1 ($x10^{+5}$) [Ω]	Q_{01} ($x10^{-7}$) [$\Omega^{-1}m^{-2}s^n$]	n_1	R_2 ($x10^{+4}$) [Ω]	Q_{02} ($x10^{-8}$) [$\Omega^{-1}m^{-2}s^n$]	n_2
	315	0,18	1,20	1,00			
	310	0,90	3,76	0,83			
	305	3,57	1,21	1,00			
	300	10,50	1,34	1,00	0,14	7,60	0,73
600	295	27,93	1,11	1,00	0,20	9,66	0,69
	290	39,00	1,18	1,00	0,30	5,12	0,72
	285				0,48	4,40	0,73
	280				0,71	3,43	0,74
	275				1,08	2,44	0,76
	315	0,29	10,08	0,74	0,15	6,77	0,71
	310	2,01	6,24	0,79	0,22	5,12	0,73
	305	4,86	4,76	0,81	0,34	5,70	0,72
	300	11,21	3,91	0,87	0,47	3,89	0,74
650	295	23,12	3,86	0,80	0,85	3,51	0,73
	290	37,10	3,17	0,93	1,06	1,81	0,78
	285	86,23	3,28	0,90	2,01	3,23	0,72
	280				3,07	1,48	0,78
	275				4,84	2,43	0,72
	315	0,11	13,64	0,84	0,05	6,75	0,75
	310	0,75	14,05	0,82	0,09	5,21	0,77
	305	2,34	9,66	0,79	0,13	3,70	0,77
	300	3,93	7,09	0,83	0,17	6,54	0,73
700	295	30,86	4,07	0,94	0,40	1,94	0,78
	290	49,56	3,16	0,95	0,69	1,76	0,78
	285				1,09	1,48	0,78
	280				1,99	1,11	0,80
	275				3,13	0,95	0,80
	315	0,65	5,78	0,68	1,80	3,38	0,72
	310	3,88	2,60	0,84	2,85	2,53	0,74
	305	7,05	2,25	0,88	4,24	2,29	0,73
	300	21,02	2,19	0,85	7,13	1,73	0,75
800	295	32,91	1,81	0,89	11,05	1,25	0,77
	290	55,64	1,63	0,87	16,78	1,07	0,78
	285				25,29	0,95	0,78
	280				37,81	0,86	0,78
	275				60,92	0,70	0,78

Table 4. Equivalent electric circuit parameters (R_1, Q_{01}, n_1, R_2, Q_{02} and n_2) for all samples at several measuring temperatures.

The values obtained by fitting the experimental data using the model of the electrical equivalent circuit shown in figure 33 (Table 4), indicate that the parameters R_1 and R_2 have similar behavior, increasing with the increase of the measurement temperature. With the increase of the TT temperature, the parameters R_1 and R_2 have a similar behavior to that observed for the dc conductivity (Table 3). The values of the Q_{01} and Q_{02} parameter decrease with the increase of the measurement temperature. Q_{01}, at room temperature, increases with the increase of the TT temperature up to 700 °C. Under these conditions, the parameter Q_{02} has an oscillatory behavior, decreasing from the sample TT600 to TT650, increasing to the sample TT700 and decreasing again to the sample TT800. The parameter n_1 decreases with increasing the measurement temperature, except for the sample TT600 that shows a value of $n_1 = 1$. At 300 K, n_1 parameter value remains substantially constant, with the increase of the TT temperature ($0.83 < n_1 < 0.87$). The parameter n_2 is almost constant for all samples, measuring conditions and TT temperatures. Note that $n_1 > n_2$, in all cases.

Based on the values of the electrical equivalent circuit parameters (Table 4) it was calculated the relaxation time (τ_Z), associated with each relaxation mechanism, and the capacitor value which best approximates the CPE element (C_{CPE}) [18]. The obtained values are in table 5. This table also presents the value of the dielectric constant and dielectric loss for all temperatures of measurement.

It is verified that the τ_{Z1} value is approximately three orders of magnitude higher than τ_{Z2}. However, both parameters decrease with the increase of the temperature of measurement for all samples, i.e., Z'' peak shifts to higher frequencies. The parameter C_{CPE1} presents a behavior similar to Q_{01} (Table 4), in function of the TT temperature, and is approximately two orders of magnitude higher than that C_{CPE2}.

9. Results analysis

The glasses with the molar compositions $92SiO_2$-$4Li_2O$-$4Nb_2O_5$ (92Si) and $88SiO_2$-$6Li_2O$-$6Nb_2O_5$ (88Si) are, due to the high amount of SiO_2, very difficult to prepare by conventional melt quenching method. However, the sol-gel method allows there preparation without major difficulties. The macroscopic aspect of the samples of these compositions depend on the presence, or absence, of inhomogeneities in the glass matrix, the particles size, quantity and refractive index [28]. In the case of the SiO_2:$LiNbO_3$ system, the refractive indices of SiO_2 (~ 1.4 [4]) and $LiNbO_3$ (~ 2.2 [29]) differ considerably. Although the translucent appearance of the as-prepared sample of the 88Si composition, the XRD pattern and SEM micrographs did not reveal the presence of heterogeneities of crystalline or amorphous nature type. The 92Si as-prepared sample is colorless and transparent. However, the results of Raman spectroscopy on the 88Si as-prepared sample showed the presence of bands centered at 240 and 680 cm^{-1}, assigned to vibrations of NbO_6 octahedrons associated with the $LiNbO_3$ structure [30;31;32;33], indicating the probable presence of small $LiNbO_3$ particles dispersed in the glass matrix. These bands are not present in the sample only subjected to the drying treatment at 120 °C, which are also transparent.

Sample	Temp. (K)	τ_{z1} ($x10^{-3}$) [s]	C_{CPE1} ($x10^{-7}$) [F]	τ_{z2} ($x10^{-6}$) [s]	C_{CPE2} ($x10^{-9}$) [F]	ε´	tan δ
	315	0,35	1,20			1873,33	0,47
	310	2,65	1,32			1722,50	0,48
	305	6,92	1,21			1585,02	0,54
	300	26,53	1,06	0,59	1,52	1330,68	0,68
600	295	51,34	1,11	0,72	1,13	1178,92	0,88
	290	75,79	1,18	0,86	0,99	1013,83	1,06
	285			1,45	1,06	859,40	1,33
	280			2,10	1,06	722,08	1,61
	275			3,10	1,08	575,66	1,84
	315	0,50	1,27	0,36	0,82	2265,03	0,89
	310	11,37	2,25	0,63	1,02	1921,36	1,86
	305	26,53	2,27	1,06	1,05	1561,59	2,06
	300	63,66	2,67	1,34	1,01	1266,14	2,36
650	295	132,63	2,42	2,50	1,03	858,17	2,62
	290	198,94	2,83	2,69	1,00	635,53	2,79
	285	454,73	3,01	6,51	1,09	384,23	2,70
	280			8,18	1,05	231,64	2,38
	275			13,84	0,98	155,36	1,93
	315	1,01	4,33	0,19	1,31	4792,50	0,97
	310	9,95	5,82	0,35	1,52	3866,72	1,97
	305	26,53	4,28	0,42	1,25	3363,29	2,59
	300	33,86	3,84	0,57	1,19	3052,55	3,07
700	295	227,36	3,73	0,90	0,89	1668,21	3,11
	290	265,26	2,93	1,56	0,89	1047,35	3,62
	285			2,35	0,86	666,41	3,83
	280			4,08	0,84	329,39	3,61
	275			6,39	0,85	188,13	2,91
	315	1,30	0,62	5,45	1,03	355,43	1,97
	310	10,61	1,24	8,72	1,09	254,31	2,10
	305	22,74	1,39	12,56	1,04	164,21	2,47
	300	61,21	1,42	20,85	1,07	92,67	2,75
800	295	88,42	1,37	29,98	1,04	62,13	2,75
	290	159,15	1,26	45,80	1,07	46,20	2,53
	285			67,78	1,05	36,99	2,20
	280			100,35	1,04	31,24	1,84
	275			147,91	0,96	26,36	1,47

Table 5. Relaxation time (τ_z) and the C_{CPE} capacitors, dielectric constant (ε´) and dielectric loss (tan δ), at 1kHz and 300 K, of the 88 Si samples.

The XRD patterns of the 88Si sample TT at 600 ºC and of the 92Si sample TT at 650 ºC, both translucent, showed that the $LiNbO_3$ crystalline phase is already formed. In the SEM micrographs of those samples it is possible to observe particles with a size that does not exceeds 500 nm, which are associated to those crystallites. The observation of particles in the 88Si sample, treated at temperatures where in the 92Si samples no particles were observed, is justified to the fact that the amount of lithium and niobium ions present in the 88Si sample is greater. As it is known, Li^+ and Nb^{5+} ions, which due to their high field strength, can promote phase separation in the vitreous network [34]. When treated at 800 °C the 88Si sample became opaque. The SEM micrographs of this sample show particles with a maximum size of 200 nm, but by XRD it was detect not only the LiNbO3 phase but also the SiO_2, and $Li_2Si_2O_5$ and Li_3NbO_4 phases. In the samples of the 92Si composition, TT at 800 °C, which are translucent, the $LiNbO_3$ and SiO_2 crystal phases are also present. Thus, the opacity of the 88Si sample, TT800, can be attributed to the presence of particles associated with the crystalline phases of $Li_2Si_2O_5$ and Li_3NbO_4.

The Li_3NbO_4 crystalline phase, present in the 88Si sample TT at 800 °C, compared with the $LiNbO_3$ phase, is richer in Li^+ ions. Thus, taking into account that the molar amount of Li^+ and Nb^{5+} ions present in the sample is equal ([Nb] / [Li] = 1), it can be confirmed the existence, in this sample, of a greater quantity of Nb^{5+} ions inserted structurally in glass matrix, than Li^+ ions. The formation of the $Li_2Si_2O_5$ crystalline phase contributes to the decrease of the number of these Li^+ ions. The absence in the Raman spectra of all the 92Si and 88Si samples, of a band at 800-850 cm^{-1} related to the vibration of the Nb-O-Si bonds, indicates that Nb^{5+} ions are probably embedded in the matrix as network modifiers. The decreasing of the number of lithium and niobium ions, structurally inserted in the glass matrix, with the increase of the TT temperature, is responsible for the decrease of the dc conductivity.

The 88Si sample, TT at 800 ºC, shows the minimum value of σ_{dc}, of all samples of this composition, indicating that this is the one that should have the smallest number of ions structurally inserted in the glass network. However, the σ_{dc} is also affected by the presence of particles, particularly those of $LiNbO_3$, which are characterized by a high resistivity (~ 10^{21} Ω. cm, at 300 K [34])

The particles observed by SEM in the sample TT800 exhibit a morphology and size similar to that observed in the samples TT at 600 and 700 °C. The detection, by Raman spectroscopy, in the samples TT at temperatures above 500 ºC, of vibrations assigned to the $LiNbO_3$ crystal structure (mainly the ones centered at 240 and 680 cm^{-1}) leads us to consider that the particles observed by SEM are $LiNbO_3$ crystallites. Knowing that the particle size is higher in the sample TT 650 than in the sample TT at 700 ºC, and that the intensity of the XRD peaks associated with the $LiNbO_3$ phase is also higher in the sample TT650, it can be assumed that the increase of the TT temperature from 650 to 700 °C promotes a dissolution of particles. Thus, the volume ratio between $LiNbO_3$ particles and the matrix glass is higher in the sample TT650 and the sample TT700 will have a larger number of Li^+ and Nb^{5+} ions structurally inserted in the glass matrix. Thus, it can be justified the observed increase of σ_{dc}

from the sample TT650 to the sample TT700. The decrease of σdc from the as-prepared glass (TT500) to the sample TT650 and from the TT700 sample to the TT800 sample is justify by a decrease in the number of charge carriers.

The 92Si samples present a σ_{dc} much lower than that observed in the 88Si samples. This difference is explained by the existence of a larger number of Li^{+} and Nb^{5+} ions, structurally inserted in the glass matrix, in the 88Si samples network.

In the 92Si samples TET at 650 °C, with amplitude lower than 500 kV/m, it were observed particles in the sample surface by SEM but not detected by XRD. This phenomenon is probably due to the fact that these particles may have a amorphous crystallinity nature. The detection by XRD, in the 650C sample and in the samples TT at temperatures above 650 °C, of $LiNbO_3$ crystal phase, indicates that the particles observed in the 650C sample surface must be associated with $LiNbO_3$.

In both compositions, and in the temperature range of the conductivity measurements, two zones with different activation energies were observed. This behavior was adjusted with an Arrhenius equation and the activation energy calculated. The only exception was the 88Si sample TT at 500 ºC. This atypical behavior can be explained considering that this sample has a microstructure with a high porosity [2]. Kincs et al. [35] found that the non-Arrhenius behavior in glasses disappears with the densification of the glass. Thus, increasing the TT temperature in the 88Si glass composition a structural densification is activated.

In all 88Si and 92Si samples, the σ_{dc} increases with the increase of the measurement temperature. This behavior, typical of a thermally stimulated process, can be attributed to the increase of the charge carriers energy, with the increase of the temperature. Assuming the ionic conductivity model, where conduction is done by the "jumps" of the charge carriers through the potential barriers [25;26;27;28], the increase of the energy of those charge carriers make their movements easier, thus increasing the σ_{dc}.

Samples of the 88Si composition show a decrease in the ac conductivity, with the increase of the TT temperature, indicating that the TT affects the structure of the glass in such way that the number of units responsible for this conduction mechanism (dipoles and/or ions) decreases or their movement, in response to the applied ac field, becomes more difficult. The $E_{a(ac)}$, calculated using the Arrhenius equation, is similar for the samples TT500, TT700 and TT800 (~ 45 kJ/mol). The remaining samples showed different $E_{a(ac)}$ values (TT600 ~ 32 kJ/mol and TT650 ~ 52 kJ/mol). The decrease of the $E_{a(ac)}$ from the sample TT500 to the sample TT600, indicates a decrease in the height of the potential barriers associated with this conduction process, suggesting that the decrease of σ_{ac} is due to a decrease in the number of dipoles, associated with lithium and niobium ions structurally inserted in the glass matrix. Considering that the particles observed in the sample TT600 are $LiNbO_3$ particles, the decreased of σ_{ac} can be explained by the formation of dipoles related with these crystals, which are difficult to depolarization [29;36] in this measuring temperatures. The sample TT650 has the highest value of $E_{a(ac)}$. This is related to the presence of $LiNbO_3$ particles agglomerates, which increases the difficulty of the associated dipoles movements. The

decrease of the σ_{ac}, from the sample TT700 to the sample TT800, is justified by the decrease of lithium and niobium ions, since both samples have similar $E_{a(ac)}$ values.

The existence of two zones with different morphology (surface and bulk), in the 92Si composition samples TET, indicate that the dielectric response can be associated to an equivalent electric circuit model as shown in figure 42.

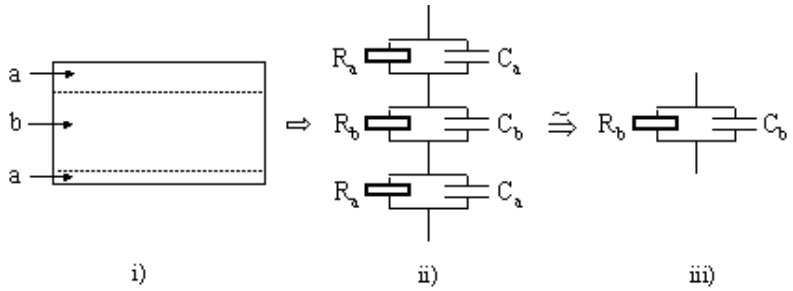

Figure 42. Equivalent electric circuit model: i) sample (a – surface; b – bulk); ii) electric model where R_a and C_a represent the resistance and the capacity related with the sample surface characteristics, R_b and C_b the resistance and capacity related to the bulk characteristics; iii) approximate model.

In the dielectric analysis, the electric circuit comes down to a combination of three capacitors in series: two related with the sample surfaces and the third with the bulk characteristics. Knowing that the thickness of the samples are about 1.0 mm, the thickness of the surface part where the particles are embedded is below 3 μm (sample 700A), the dielectric constant (ε ') of $LiNbO_3$ is higher than 10^3 at 300 K and 1 kHz [29], being much higher than the ε ' of the bulk sample zone, assumed to consist mainly of glass matrix ($\varepsilon'_{SiO_2} \approx 4.0$), it is reasonable to consider that the dielectric behavior can be controlled by the characteristics of the bulk. Briefly, the analysis of the electrical circuit consisting of three capacitors in series shows that the equivalent capacity is

$$C_{eq} = \frac{C_a C_b}{C_a + 2C_b}$$

If we consider that $C_a >> C_b$ than $C_{eq} \approx C_b$. Therefore the increase of ε' in the samples series treated at 750 ° C, with the increase of the external electric field amplitude may be associated with an increase in the number of dipoles present in the bulk region of the samples. In these samples it was observed a decrease in the $LiNbO_3$ particle size, with the increase of the applied electric field amplitude. This reduction is also associated with the decrease of intensity of the Raman band centered at 630 cm^{-1} related to the presence of $LiNbO_3$ particles [24], indicating a decrease in the number of dipoles associated with those particles. By increasing the electric field amplitude applied during the heat treatment, the σ_{dc} increases. This behavior must be related to the presence of a higher number of Li^+ and Nb^{5+} ions inserted structurally in the glass matrix. Thus it can be assumed an increase in the number of electric dipoles in the bulk zone with the increase of the amplitude of the electric field.

In the samples series TET at 700 °C, the behavior of ε', with the increase of the external electrical field amplitude, is opposite to the one observed in the samples TET at 750 °C. The increase of the particle size in the samples TET at 700 °C, with the increase of the external electrical field amplitude, was observed by SEM and by Raman spectroscopy (increase of the intensity of the band centered at 630 cm^{-1}). This fact will cause a reduction in the number of dipoles in the sample bulk zone, thereby reducing the ε' value. The same occurs in the sample TET at 650 °C. Thus, these results suggest that in the samples TET at 650 °C and 700 ºC the Nb5+ and Li^+ ions migrate from the bulk zone to the surface, contributing to the increase of the particles size.

The dielectric response, using the impedance formalism (Z*), as a function of frequency and temperature for the 92Si composition samples was adjusted to the physical model consisting on the equivalent circuit shown in figure 43 [R_1(RCPE_1)].

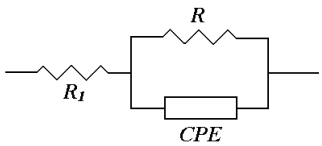

Figure 43. Equivalent electric circuit model.

It is noted that this model fits the experimental data reasonably, showing for all the samples a value of the parameter n very close to 1 (> 0.9), indicating that CPE element behaves very close to a capacitor. The value of R_1 ~0 was considered in all samples.

In the 88Si composition samples it was detected two relaxation mechanisms, which were fitted, using the CNLLS algorithm, to the equivalent circuit model shown in figure 33 ([R_0($R_1$$CPE_1$)($R_2$$CPE_2$)]). From the obtained values, it should be noted that the parameters n_1 and n_2, associated to the elements and CPE_1 and CPE_2, respectively, are always higher than 0.73, which shows that also in this composition, the elements CPE tend to exhibit a behavior similar to a capacitive element. The relaxation mechanism, found in the high frequency region ($R_2$$CPE_2$) is assigned to the characteristics of the vitreous matrix ("bulk"), i.e., with the relaxation of dipoles associated with the ions structurally inserted in the glass matrix. The relaxation at the lowest frequencies was associated with surface features, namely those related with the dipoles related with the particles detected at the samples surfaces. The presence of those particles, related with the $LiNbO_3$ crystalline phase, which is characterized by possessing dipoles which electrical depolarization is difficult, justifies the higher relaxation time. The fact that the relaxation time associated with the first depolarization mechanism, observed in the 88Si composition, is of the same order of magnitude to that observed in the 92Si samples composition, suggests that the electrical units responsible for both are the same, i.e., the dipoles associated with lithium and niobium ions inserted structurally in the glass matrix. In the 88Si composition, the relaxation time τ_{Z1}, related with the $R_1$$CPE_1$, and associated with the relaxation mechanism at the low frequency zone, is higher (~ 10^{-2} s) than the τ_{Z2}, which also indicates that the units responsible for this relaxation are more difficult to depolarize.

In the 92Si composition, the Z* behavior as a function of frequency, for the TET samples treated at 700 ºC is opposite to that observed in the samples TET at 750 ºC, with the increase of the external electric field amplitude (the series TET at 650 and 700 ºC have a similar behavior). In the samples TET at 750 ºC, the increase of the amplitude of the external electrical field, promote an increase in the values of the R and Y0 parameters. This behavior should be associated with the increase of the number of particles in the sample bulk zone. In the samples TET at 650 and 700 °C, the number of electrical units within the sample (bulk region) decreases with the increase of the amplitude of the external electrical field, and therefore, increases the number of surface particles, justifying the Z*(ω) opposite behavior.

The 92Si composition presents dielectric constant (ε ') and dielectric loss (tan $\delta = \varepsilon'' / \varepsilon'$) values, much lower than those observed in the 88Si composition samples. The justification for this value disparity is the larger number of electric dipoles existing in the 88Si composition sample. In this composition, the decrease of ε', from the sample TT at 600 ºC to the sample TT at 650 ºC, measured at room temperature and 1 kHz, is due to the presence, in the sample TT650, of particle agglomeration and also to high size particles, which promotes the decrease of the number of dipoles associated with lithium and niobium ions structurally inserted in the glass matrix. Furthermore it is likely that the crystal orientation of the particles and agglomerates, do not present a preferential grow direction contributing to the decrease of the dipole moment [36;37].

The parameter tan δ (92Si composition) increases in the samples TET at 750 °C, with the increase of the amplitude of the external electrical field, mainly due to the increase of the ε'' component. This behavior will cause an increase in the conductivity, which is corroborated by the R parameter behavior. The decrease in the value of τ_Z, in the samples TET at 750 °C with the increase of the amplitude of the electric field, suggests that the electrical units, present in these samples, follow the ac electric field more easily. In the TET samples treated at 650 °C, the behavior of tan δ (with increasing the amplitude of the external electric field) is opposite to that observed in the samples TET at 750 °C. This can be attributed to a significant increase in the ac resistivity. Moreover ε' decreases due to the increase of the surface particles amount and thus reducing the amount of ions in the glass bulk zone.

The presence in samples of the 88Si composition of two relaxation peaks, in the Z* spectrum, similar to those already observed in other glass containing $LiNbO_3$ crystals [38;39;40] suggests that the dc conductivity at low temperature and the dielectric relaxation at high-frequency can be assigned to the ion conduction and ionic polarization, respectively. The σ_{dc} behavior at temperatures higher than 300 K and the relaxation process in the low frequency range should be assigned to interfacial electrode-sample polarization [38;39;40].

10. Main conclusions

1. The sol-gel method allows the preparation of glasses and glass ceramics with compositions that by the melt-quenching method are extremely difficult to prepare.

2. The drying process keeps the 92Si composition gel transparent and the 88Si translucent. The heat treatment with or without the presence of the external electrical field, makes the 92Si glass composition translucent. Samples of the 88Si composition, after TT at temperatures above 750 ºC, became opaque.
3. The detection of $LiNbO_3$ crystal phase is observed in the 92Si sample composition TT at temperatures above 650 °C and in the 88Si composition at temperatures above 600 °C. Increasing the annealing temperature it is promoted the appearance of secondary crystalline phases.
4. SEM revealed that crystallization in both 92Si and 88Si compositions are predominantly at the glass surface.
5. Samples of the 92Si composition, TET at temperatures below 650 ºC, promote the formation of $LiNbO_3$ crystallites
6. Increasing the amplitude of the electric field in the 92Si sample series treated at 650 and 700 °C favors the increase in the particle size. The TET at 750 ºC presents the opposite behavior.
7. The decrease in the surface particle size associated with an increase in the number of dipoles within the sample, justifies the maximum value of ε' observed (9,44). Thus, the study of the dielectric constant enables to establish if the crystallization occurs, preferably in the sample surface or in the bulk zone.
8. The high values of ε', measured in the low frequency region (<1 kHz) in the 88Si samples, are due to interfacial polarization. The increase in the amount of surface particles promotes a decrease of ε', indicates that these particles grow without a preferential crystalline orientation.
9. The 88Si composition sample treated at 650 °C shows particle agglomerates that are dissolved, with increasing the thermal treatment temperature. This structural change is substantiated by the SEM results and by the decreasing of the width and increasing of the intensity of the Raman bands. The results of σdc strengthen the hypothesis that the formation of secondary phases ($Li_2Si_2O_5$ and Li_3NbO_4), in the 88Si samples composition comes from the dissolution of the $LiNbO_3$ agglomerated particles.
10. The results of the Raman spectroscopy indicate that the niobium ions are inserted in the glass matrix as network modifiers.
11. The samples of these two compositions present two different temperature zones with different activation energies indicating the presence of two different conduction mechanisms. In the samples of the 88Si composition it was also detected the presence of two dielectric relaxation mechanisms. The $E_{a(dc)}$ associated with the region of low temperatures and the dielectric relaxation mechanism associated with the high frequency region are assigned to ionic conduction and ionic polarization, respectively. The relaxation mechanism observed in the low frequency region and the $E_{a(dc)}$ associated with the region of high temperatures, are due to interfacial polarization phenomena.
12. The CNLLS algorithm associated with an electrical equivalent circuit model was used to adjust the dielectric behavior. The detection of two different relaxation mechanisms in the 88Si samples led to the use of the electrical equivalent circuit shown in figure 41. The results obtained by fitting the experimental data showed that this model may describe the dielectric behavior of these samples.

Author details

Manuel Pedro Fernandes Graça and Manuel Almeida Valente
University of Aveiro / I3N - Physics Department, Portugal

Acknowledgement

The authors gratefully acknowledge the financial support from PEst-C/CTM/LA0025/2011 and from the Portuguese Science and Technology Foundation (FCT) - SFRH/BD/6314/2001.

11. References

[1] Mauritz, www.psrc.usm.edu/~mauritz/sol-gel.html (2002).
[2] I. Schwartz, P. Anderson, H. de Lambilly, L.C. Klein, J. Non-Cryst. Solids, 83, 391-399 (1986).
[3] E.O. Lawrence, Berkeley National Laboratory, "How silica aerogels are made", in http://eande.lbl.gov/ECS/aerogels/saprep.htm .
[4] J.M.F. Navarro, "El Vidrio" (CSIC-Fundación Centro Nacional del Vidrio, Madrid 1991).
[5] S. Sakka, "Treatise on materials science and technology", vol 22, Academic Press, 1982.
[6] F. Mehran, B.A. Scott, Solid State Communications, 11, 15-19 (1972).
[7] M. G. Ferreira da Silva, "Incorporação Estrutural de Iões de Transição em Vidros Preparados pelo Método Sol-Gel", PhD thesis, Universidade de Aveiro, Portugal (1990).
[8] I.M.M. Salvado, "Preparação pelo processo "Sol-Gel" e caracterização de materiais dos sistemas SiO2-ZrO2, SiO2-TiO2, SiO2-Al2O3. Aplicação como revestimentos protectores."- PhD thesis, Universidade de Aveiro, Portugal (1990).
[9] N. Venkatasubramanian, B. Wade, P. Desai, A S. Abhiraman, L.T. Gelbaum, 130, 144-156 (1991).
[10] L.C. Klein, S. Ho, "Glasses for electronic applications", (1991) 221-233.
[11] S.P. Szu, M. Greenblatt, L.C. Klein, Solid State Ionics, 46, 291-297 (1991); S.P. Szu, L.C. Klein, M. Greenblatt, J. Non-Cryst. Solids, 143, 21-30 (1992).
[12] C. Sanchez, G.A.A. Soler-Illia, F. Ribot, D. Grosso, C.R. Chimie 6 (2003), 1131-1151.
[13] K. Chou, J. Non-Cryst. Solids, 110 (1989) 122-124.
[14] M. Prassas, "Silica Glass from Aerogels", in http://www.solgel.com/articles/april01/aerog2.htm .
[15] R. Ota, N. Asagi, J. Fukunaga, N. Yoshida, T. Fujii, J. Mat. Sci., 25, 4259-4265 (1990).
[16] M.P.F. Graça, M.G.F. Silva, M.A. Valente , Journal of Non-Crystalline Solids, 351 (33-36) (2005) 2951-2957.
[17] MPF Graça, MGF Silva and MA Valente, Journal of Sol-Gel Science and Technology, 42 (1) (2007) 1-8.
[18] Manuel Pedro Fernandes Graça & Manuel Almeida Valente, Glass Ceramics with Para, Anti or Ferroelectric Active Phases – book chapter 11 (pp213-292) in: Ceramic Materials", ISBN: 978-953-307-217-3, Intech publisher, 2011.

[19] MPF Graça, MGF Silva, ASB Sombra and MA Valente, Journal of Non-Crystalline Solids, 352 (42-49) (2006) 5199-5204.
[20] T. Cardinal, E. Fargin, G. Le Flem, S. Leboiteux, J. Non-Cryst. Solids 222 (1997) 228-234.
[21] A.C:V de Araujo, I.T. Weber, W.D: Fragoso, C.M. Donegá, J. of Alloys and Compounds 275-277 (1998) 738-741.
[22] Y.D. Juang, S.B. Dai, Y.C. Wang, W.Y. Chou, J.S. Hwang, M.L. Hu, w.S. Tse, Solid State Communications 111 (1999) 723-728.
[23] N. Shibata, M. Horigudhi, T. Edahino, J. Non-Cryst. Solids, 45 (1981) 115-126.
[24] A A Lipovskii, V.D. Petrikov, V.G. Melehin, D.K. Tagantsev, B.V. Tatarintsev, Solid State Comunications, 117, 733-737 (2001).
[25] J.R. Macdonald, "Impedance spectroscopy", John Wiley & Sons, New York, 1987.
[26] M.P.F. Graça, M.A. Valente, M.G. Ferreira da Silva, Journal of Materials Science, 41 (4) (2006) 1137-1141.
[27] A.K. Jonscher, "Dielectric relaxation in solids", Chelsea Dielectrics Press, London, 1983.
[28] H.G. Kim, T. Komatsu, R. Sato and K. Matusita , J. Non-Cryst. Solids, 162, 201-204 (1993).
[29] M.M. Aboulleil, F.J. Leonberger, J. Am. Ceram. Society, 72 (1989) 1311-1320.
[30] R.Claus, G.Borsel, E. Wiesendanger, L.Steffan, Phys. Ver. B, 6(12) (1972) 4878-4879.
[31] A. Jayaraman, A. A. Ballman, J. Appl. Phys., 60 (3) (1986) 1208-1210.
[32] J.G. Scott, S. Mailis, C.L. Sones, R.W. Eason, Appl.Phys. A, 2003.
[33] A. Ridah, P. Bourson, M.D. Fontana, G. Malovichko, J. Phys. Condens. Matter 9 (1997) 9687-9693.
[34] W. Vogel, Glass Chemistry, Springer, 2nd edition, 1994.
[35] J. Kincs, S. W. Martin, Physical Review letters, 76 (1) (1996) 70-73.
[36] MPF Graça, MGF Silva and MA Valente, Journal of Materials Science, 42(8) (2007) 2543-2550.
[37] Glasses with ferroelectric phases, M.A. Valente and M.P.F. Graça, IOP Conf. Series: Materials Science and Engineering 2 (2009) 012012.
[38] E.B. de Araujo, J.A.M. de Abreu, R.S. de Oliveira, J.A.C. de Paiva, A.S.B. Sombra, Canadian Journal of Physics, 75 (1997) 747-758.
[39] C. Hong, D.E. Day, J. Mater. Sci., 14, 2493-2499 (1979).
[40] C. Hong, D.E. Day, J. Am. Ceram. Soc., 64:2, 61-67 (1981).